Conformation and Dynamics of Cellulosic and Amylosic Chains in Solution

A Doctoral Thesis

by

Xinyue Jiang

Submitted to

the Graduate School of Science, Osaka University

May, 2017

Acknowledgement

This thesis work was carried out from 2014 to 2016 under the direction of Professors Takahiro Sato at the Department of Macromolecular Science, Graduate School of Science, Osaka University. I express my sincerest gratitude to Professors Takahiro Sato for his kindest guidance, valuable suggestions and discussions during this work. I also would like to extend my gratitude to associate Professor Ken Terao, and Professor Tadashi Inoue for their helpful advice and valuable discussions.

I would like to express my deep gratitude to Professor Atsushi Nakagawa at the Institute for Protein Research, Osaka University for his careful review and valuable comments.

I would like to gratefully acknowledge Professor Shinichi Kitamura (Graduate School of Life and Environmental Sciences, Osaka Prefecture University) for his kind provision of amylose samples and valuable comments.

I am grateful to Mr. Rintaro Takahashi in the Sato laboratory for SAXS measurements and Mr. Ryoki Akiyuki for cellulose tris(n-octadecylcarbamate) measurements, Mr. Atushi Matumoto and Mr. Yuki Okada in the Inoue laboratory for viscoelastic measurements, and Maeda Ayaka (National Institute of Advanced Industrial Science and Technology) for her helpful advice.

Finally, I express my sincerest thanks to my family members and friends for their constant support and warmest encouragements.

May, 2017

蔣昕悅

Xinyue Jiang

Contents

Chapter I.

General Introduction

I-1. Conformation and Dynamics of Polymer Chains

Physical properties of polymeric materials are governed by the conformation and dynamics of the polymer chain in the materials. Thus, in order to apply polymer materials in the best condition, it is important to understand the conformation and dynamics of the polymer chain. However, it is not the easy task because of the polymer-chain complexity, as mentioned below.

As shown in Figure I-1, a linear chain molecule consisting of $n + 1$ main-chain atoms with fixed bond lengths b and bond angles θ has $n + 4$ degrees of freedom: six external (translational and rotational) degrees of freedom and $n - 2$ internal rotations. The conformation of this linear chain polymer is specified by the $n - 2$ internal rotation angles. The global and local dynamics of the polymer chain is described by time evolutions with respect to the six external and $n - 2$ internal degrees of freedom, respectively. Thus, if n is large, both conformation and dynamics of the polymer chain becomes very complex. To overcome this complexity, polymer physicists proposed various course-grained polymer chain models, as explained below.

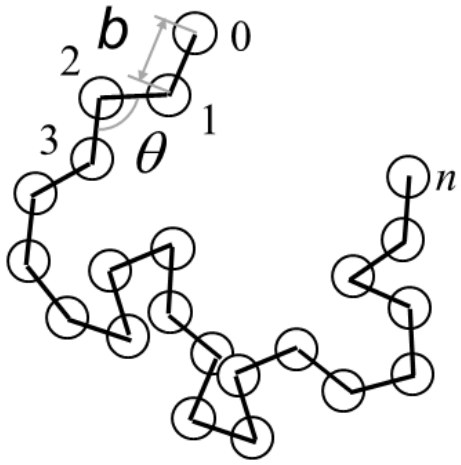

Figure I-1. A schematic diagram of a linear chain polymer.

I-2. Various Polymer Chain Models

I-2-1. Gaussian Chain Model

The polymer chain in Figure I-1 is divided into n_s sub-chains (cf. Figure I-2). If n/n_s is large enough, the distribution function with respect to the end-to-end vector **r** of the sub-chain obeys the Gaussian function[1, 2]

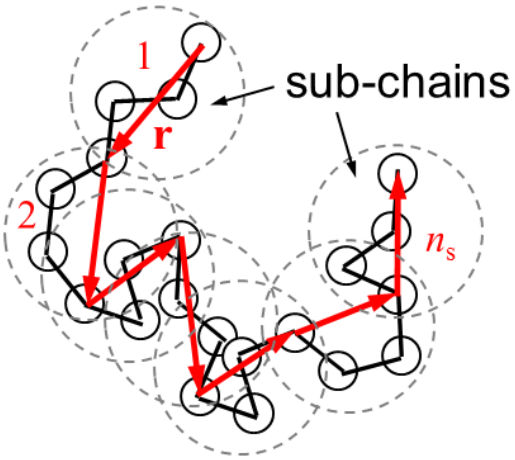

Figure I-2. A schematic diagram of the Gaussian chain model (red arrows).

$$P(\mathbf{r}) = \left[\frac{3}{2\pi\left(n/n_s\right)C_\infty b^2}\right]^{3/2} \exp\left[-\frac{3r^2}{2\left(n/n_s\right)C_\infty b^2}\right] \qquad \text{(I-1)}$$

where r is the magnitude of $\mathbf{r}$, b is the bond length, and C_∞ is the characteristic ratio of the polymer chain, which is calculated in terms of the bond angle θ and the internal rotation potential. The sequence of the above n_s sub-chains is called as the Gaussian chain model. This model was first introduced by Kuhn[3, 4] to describe the conformation of flexible polymers. The mean square end-to-end distance $\langle R^2 \rangle$ of the Gaussian chain is given by

$$\langle R^2 \rangle = n_s \int r^2 P(\mathbf{r}) \mathrm{d}\mathbf{r} = n_s \left(n/n_s\right) C_\infty b^2 = n C_\infty b^2 \qquad \text{(I-2)}$$

The intrinsic viscosity [η] is related to the end-over-end rotation of the polymer chain in the solvent. Kirkwood and Riseman[5] formulated this hydrodynamic quantity of the global chain dynamics using the Gaussian chain model. The result is written as

$$[\eta] = \Phi \frac{\langle R^2 \rangle^{\frac{3}{2}}}{M} \qquad \text{(I-3)}$$

where Φ is called as the Flory viscosity constant (= 2.87×10^{23} mol^{-1}), and M is the molar mass of the polymer. This equation demonstrates the direct relation between the conformation and global (slow) dynamics of the polymer chain. Kirkwood and Riseman[5] also demonstrated similar direct relations of the translational and rotational frictional coefficients to $\langle R^2 \rangle$.

I-2-2. Bead-Spring Model

According to the statistical mechanics, the Helmholtz energy $F(\mathbf{r})$ of the Gaussian sub-chain at a given $\mathbf{r}$ is expressed in terms of $P(\mathbf{r})$ as

$$F(\mathbf{r}) = -k_{\mathrm{B}}T \ln\left[ZP(\mathbf{r})\right] \tag{I-4}$$

where $k_{\mathrm{B}}T$ is the Boltzmann constant, T is the absolute temperature, and Z is the partition function with respect to the polymer chain conformation. When $\mathbf{r}$ is enlarged, the elastic force $\mathbf{f}$ is induced between both chain ends to reduce $F(\mathbf{r})$. This force is referred to as the entropic elasticity. Using eqs I-2 and I-4, $\mathbf{f}$ is given by

$$\mathbf{f} = \frac{\partial F(\mathbf{r})}{\partial \mathbf{r}} = \frac{3k_{\mathrm{B}}T}{(n/n_{\mathrm{s}})C_{\infty}b^2}\mathbf{r} \tag{I-5}$$

This equation indicates that the Gaussian sub-chain can be regarded as an elastic spring according to the Hooke law, where the elastic force constant is given by $3k_{\mathrm{B}}T/(n/n_{\mathrm{s}})C_{\infty}b^2$.

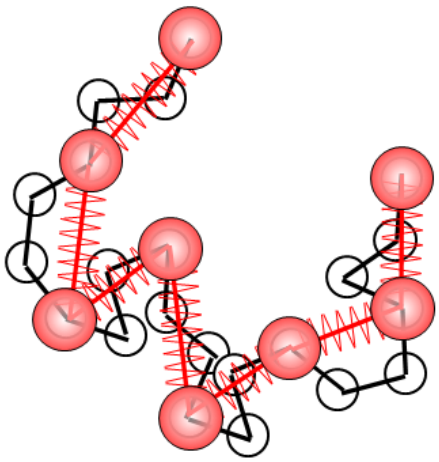

Figure I-3. A schematic diagram of the bead-spring model.

The bead-spring model views the polymer chain shown in Figure I-1 as the sequence of n_s elastic springs, and $n_s + 1$ beads are attached to all junctions between neighboring springs and the chain ends as friction points against the solvent (cf. Figure I-3). The bead-spring model was first introduced by Rouse[6] to formulate both global and local polymer chain dynamics. The sub-chain or the spring is referred to as the Rouse segment. The Rouse segment length b_s is given by

$$b_s = \sqrt{(n/n_s)C_\infty}\, b \tag{I-6}$$

Including the intramolecular hydrodynamic interaction, Zimm[7] derived the same equation as eq I-3 for $[\eta]$ using the bead-spring model under the shear flow at the zero shear rate. On the other hand, under the oscillatory flow, the bead-spring model shows the viscoelastic response characterized by the complex modulus[6, 7]

$$G^*(\omega) = \frac{cRT}{M}\sum_{p=1}^{n_s}\frac{\mathrm{i}\omega\tau_p}{1+\mathrm{i}\omega\tau_p}, \quad \tau_p = \frac{\tau_{RZ}}{p^k} \quad (1.5 \le k \le 2) \tag{I-7}$$

where c is the polymer mass concentration, R is the gas constant, ω is the angular frequency of the oscillatory flow, and τ_{RZ} is the relaxation time of the end-over-end rotation of the whole chain. Equation I-7 provides us the storage modulus $G'(\omega)$ and the loss modulus $G''(\omega)$ illustrated in Figure I-4.

In the high frequency limit, the storage modulus tends to

$$G'(\infty) = \frac{cRT}{M_s} \tag{I-8}$$

where M_s (= M/n_s) is the molar mass of the Rouse segment, characterizing local dynamics of the polymer chain in solution. In the low frequency limit, the slope of the loss modulus is equal to $\eta_S[\eta]M/RT\tau_{RZ}$, where η_S is the solvent viscosity.

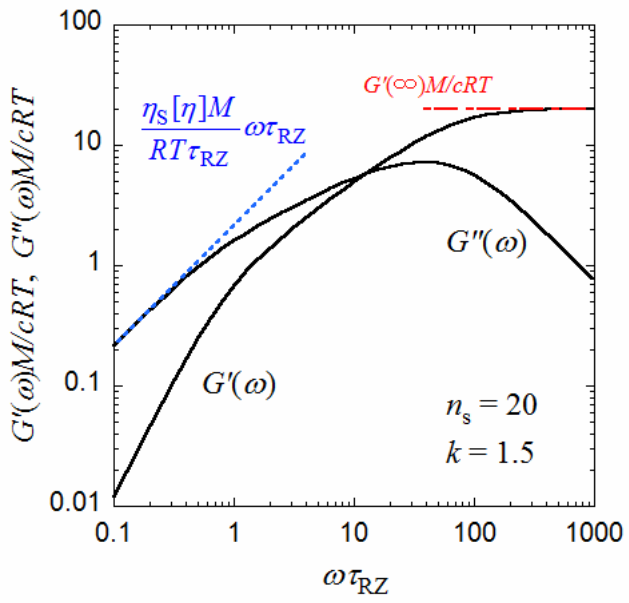

Figure I-4. Storage and loss moduli of the Rouse chain.

I-2-3. Wormlike Chain Model

If the number of bonds n/n_s per sub-chain is not sufficiently large, $P(\mathbf{r})$ and b_s of the sub-chain (or the Rouse segment) do not obey any more eqs I-1 and I-6, respectively. This is the chain stiffness effect. To take this effect into account, Kratky and Porod[8] introduced the wormlike chain model, which is viewed as a microscopic elastic wire, as shown in Figure I-5.

The wire can be specified by the contour length L and the bending force constant ε, or the Kuhn segment length λ^{-1} defined by[2, 9]

$$\lambda^{-1} = \frac{2\varepsilon}{k_{\mathrm{B}}T} \tag{I-9}$$

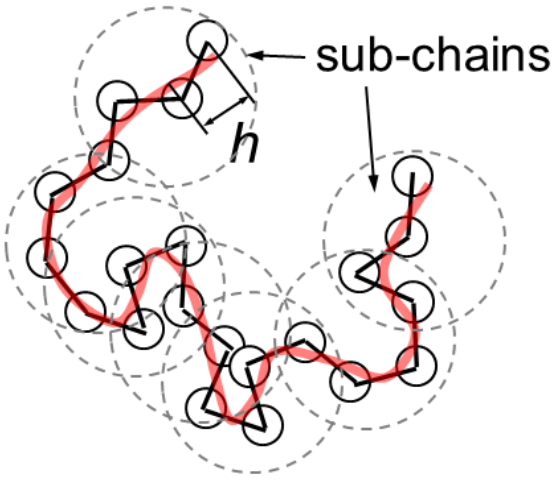

Figure I-5. A schematic diagram of the wormlike chain model (red curve).

The energetically most stable conformation of the wormlike chain is the straight rod conformation without any bending. On the other hand, the corresponding conformation of the conventional bond model shown in Figure I-1 depends on the internal rotation potential energy function. For example, for vinyl polymers of which main chain consists of carbon-carbon single bonds, the all trans zigzag conformation is energetically most stable. Therefore, the straight rod conformation of the wormlike chain must be identified with the all trans zigzag conformation of the conventional bond model for vinyl polymers, from which we have the following relation:

$$L = nh = nb\sin\left(\theta/2\right) \tag{I-10}$$

Here, h is the projection length of the bond vector onto the trans zigzag chain axis (cf. Figure I-5), corresponding to the wormlike chain contour. For helical polymers, h corresponds to the helix pitch per bond.

According to the wormlike chain statistics, $\langle R^2 \rangle$ is written as[2]

$$\langle R^2 \rangle = \lambda^{-1}L - \frac{1}{2}\lambda^{-2}\left(1 - \mathrm{e}^{-2\lambda L}\right) \tag{I-11}$$

When the Kuhn segment number λL is sufficiently large, the chain stiffness effect can be neglected, and eq I-11 reduces to eq I-2, where we have the following relation between the two chain models

$$\lambda^{-1} = C_\infty \frac{b^2}{h} \tag{I-12}$$

When the wormlike chain is divided into n_s sub-chains, the distribution function of the end-to-end vector $\mathbf{r}$ of the sub-chain is approximately given by[10]

$$P(\mathbf{r}) = \left(\frac{3n_s}{2\pi\lambda L}\right)^{3/2} \exp\left(-\frac{3\lambda n_s r^2}{2L}\right)\left(1 - \frac{5n_s}{8\lambda L} + \frac{2{n_s}^2 r^2}{L^2} - \frac{33\lambda {n_s}^3 r^4}{40L^3}\right) \tag{I-13}$$

using the first Daniels approximation. The elastic force f of the sub-chain is calculated from eqs I-4 and by

$$f = \frac{3\lambda n_s}{L} k_B T\left[1 - \frac{4}{3}\left(\frac{M_s}{M_K}\right)^{-1} - \frac{5}{6}\left(\frac{M_s}{M_K}\right)^{-2} - \frac{25}{48}\left(\frac{M_s}{M_K}\right)^{-3}\right] r \tag{I-14}$$

where eqs I-6, I-10, and I-12 were used, and M_K is the molar mass per the Kuhn segment length defined by

. $$M_K = \lambda^{-1}\frac{M}{L} = \lambda^{-1}M_L \qquad \text{(I-15)}$$

(M_L: the molar mass per unit contour length). As shown in Figure I-6, the elastic force constant **f/r** decreases with decreasing M_s/M_K due to the chain stiffness effect. If the chain stiffness effect on the Rouse segment becomes important, the junction between neighboring springs cannot be regarded as the free joint, and the basic assumption of the Rouse model breaks down. Therefore, M_s must be so high that the chain stiffness effect is less important. However, if M_s is too high, the Rouse model cannot describe the local chain dynamics. Thus, M_s must be chosen so as to fulfill these two requirements.

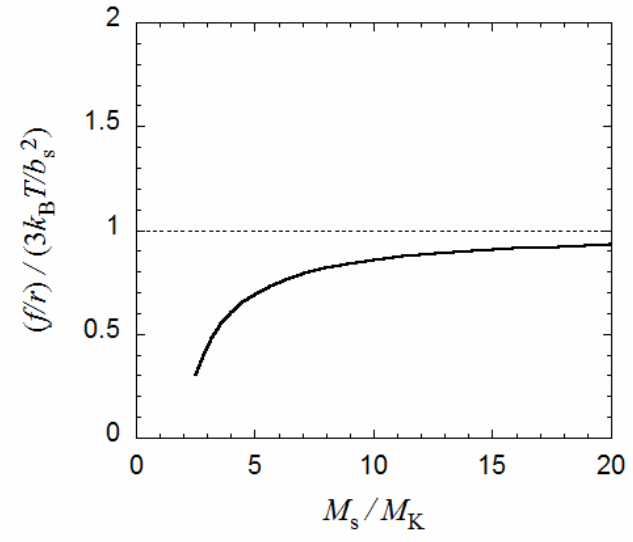

Figure I-6. Chain stiffness effect on the spring force constant.

1-3. Previous Studies on the Conformation and Local Dynamics of Polymer Chains in Solution

1-3-1. Polystyrene

The conformation of flexible polymers used to be analyzed by the Gaussian chain model by 1970's was treated without the chain stiffness effect.[2] In 1990's, the Kuhn segment lengths λ^{-1} for such flexible polymers were determined by the comparison of dilute solution properties (the radius of gyration, intrinsic viscosity, hydrodynamic radius, and so on) of low molecular weight samples, where the chain stiffness effect becomes important, with the wormlike or helical wormlike chain model.[11] For example, λ^{-1} for polystyrene was estimated to be ca. 2 nm in cyclohexane and toluene.[11, 12] The molar mass of the Kuhn segment M_K is calculated to be 830 g/mol.

To obtain the storage modulus $G'(\infty)$ in the high frequency limit, rheological and rheo-optical measurements must be carried out at $\omega\tau_{ns} >> 1$ (cf. eq I-7). Because τ_{ns} is proportional to the solvent viscosity, one must use a viscous solvent for the measurements to fulfill the condition $\omega\tau_{ns} >> 1$. For polystyrene, chlorinated diphenyls (Aroclors) and tricresyl phosphate (TCP) were used as such solvents.[13, 14] The result of M_s was reported to be ca. 5000 g/mol in dilute solutions. This indicates that the internal motion within 50 monomer units of polystyrene does not contribute to fast rheological and rheo-optical properties.

The previous results of λ^{-1} and M_s were obtained in the different solvents, because it is experimentally difficult to determine λ^{-1} in such viscous solvents. Amelar et al. [13] however demonstrated that the intrinsic viscosities and the translational diffusion coefficients of polystyrene in Aroclors, toluene, and cyclohexane are indistinguishable. This indicates that λ^{-1} values of polystyrene in Aroclors is identified with those determined in toluene and cyclohexane (= ca. 2 nm), and the ratio M_s/M_K for polystyrene is ca. 6 in Aroclors. As shown in Figure I-6, the entropic elastic force constant diminishes to 75 % at M_s/M_K = 6 by the chain stiffness effect. Therefore, the level off of $G'(\omega)$ of polystyrene in the high frequency limit is at least partly owing to the chain stiffness effect of polystyrene.

1-3-2. Cellulose and Its Derivatives

Figure I-7 shows the chemical structures of cellulose. Cellulose consists of D-glucose residues. To argue its chain conformation, each glucose residue is represented by the virtual bond **b** between neighboring glycosidic bond oxygen atoms shown in Figure I-7 (dotted arrows), and those oxygen atoms should be regarded as circles in Figure I-1. The orientation of the virtual bond is determined by two internal rotation angles ϕ and ψ in the figure, and the virtual bond angle θ can vary by changing ϕ and ψ.

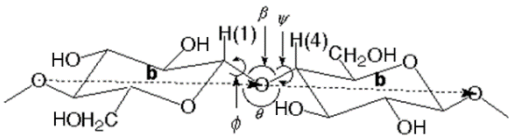

Figure I-7. Chemical structure and the virtual bond of the cellulosic chain.

Because cellulose has many hydroxyl groups forming intermolecular hydrogen bonds, it is difficult to dissolve cellulose in common organic and inorganic solvents. Thus, to dissolve cellulose, one must use hydrogen-bond breaking solvents or modify chemically cellulose by substituting hydroxyl groups of cellulose.

Copper complex with ammonia (cuoxam) was invented by Schweitzer in 1857 as the first known solvent for cellulose.[15] Afterwards, there were many reports of other alternatives of aqueous alkaline solutions and also of hydrogen-bond breaking non-aqueous solvents (e.g., dimethylsulfoxide and dimethylacetamide) as the solvent for cellulose. In 2002, Rogers et al. reported that ionic liquids were capable of dissolving cellulose at high concentrations.[16] Ionic liquids compose of a salt with halide counter ions such as 1-butyl-3-methyl-imidazolium chloride (BmimCl) and 1-allyl-3-methylimidazolium chloride (AmimCl), and other counter anions such as phosphate[17], formate[18] and acetate[19]. It becomes clear that the hydrogen bond accepting ability of anion plays a dominant role on cellulose dissolution process. Due to their high viscosities, it is rather difficult to use ionic liquids as the solvent for charactering the conformation of cellulose, but useful for high frequency rheological and rheo-optical

measurements.

Schoenbein reported the formation of cellulose nitrate in a HNO_3-H_2SO_4 component solvent around 1846.[20] In the same year, F. J. Otto produced the guncotton and was the first to publish the process.[21] Afterwards, there were many reports that cellulose esters, ethers, and carbamates dissolve in common organic solvents, dilute solution studies were carried out to characterize the conformation of the cellulosic chain.

Cellulose and its derivatives are known to possess the chain-stiffness between typical flexible and stiff polymers. Due to this intermediate chain stiffness, there were historical disputes as to whether the extended chain conformation of cellulose comes from the intra-molecular excluded volume effect or the chain stiffness effect in 1960's.[22, 23] After Yamakawa et al.[11] developed the quasi-two-parameter theory for the excluded volume effect on the basis of the (helical) wormlike chain model in mid-1980's, λ^{-1} values of cellulose and its derivatives were determined in various solvents by taking the excluded volume effect into account.

Recently, Maeda et al.[24] made rheological and rheo-optical measurements for ionic liquid solutions of cellulose to determine M_s. Their result of M_s for cellulose in BmimCl was 2300 g/mol, and M_s was almost independent of polymer concentration. Maeda [25] also made light scattering measurements on cellulose dissolved in an ionic liquid, but because of the high viscosity, low light-scattering power, and fluorescence of the test solution, the value of λ^{-1} obtained contained a considerable experimental error.

1-3-3. Amylose and Its Derivatives

Amylose is another polymer of D-glucose, with the glycosidic bonding different from that of cellulose. The chemical structure of amylose is illustrated in Figure I-8. Due to the α-linkage of the glycosidic bond, the potential map with respect to the internal rotation angles ϕ and ψ in the figure is considerably different from that of cellulose, which reflects on the chain stiffness.

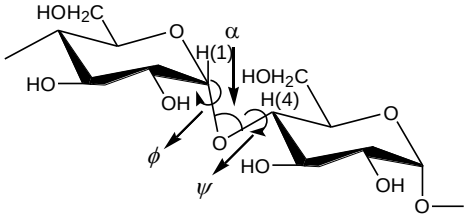

Figure I-8. Chemical structure and the virtual bond of the amylosic chain.

Amylose samples extracted from native starch are not suitable to investigate their conformational properties quantitatively in solution because of their branching structure .[26] In 1986, Waldmann et al.[27] reported that amylose samples with no branch and furthermore narrow molar mass distributions can be synthesized enzymatically, which is suitable to study the conformation of the amylosic chain. Mainly due to more flexible nature than cellulose, amylose can dissolve in various common polar organic and inorganic solvents, and λ^{-1} of amylose in such solvents was determined to be 2 – 4 nm, or 4 nm.[28-30] Only the exception is λ^{-1} = 18 nm in aqueous iron-sodiumtartrate.[31, 32]

Terao et al.[33-36] extensively studied the chain conformation of various amylose carbamates in various organic solvents. The rigidity of amylose carbamate derivatives is widely distributed from 9 nm to 75 nm. Furthermore, the helix pitch (or helix rise) per residue *h*, which does not change so much in most polymers, changes considerably from 0.25 nm to 0.42 nm. This change in *h* reflects the change in the helical structure of the amylose chain. One of the reasons for the high rigidity of the amylose carbamate derivative is the intramolecular hydrogen bond between the NH group of the substituent and the C=O group.

Maeda[18] studied the Rouse segment size not only for cellulose but also for amylose in the ionic liquid BmimCl by rheological and rheo-optical measurements. The M_s value obtained was 2200 g/mol at the amylose concentration of 3 wt%. However, she did not study the conformation of amylose in BmimCl.

I-4. Scope of This Work

The aim of this thesis is to investigate the relation between the conformation and local dynamics of polymer chains with different chain stiffness. The local chain dynamics is studied by rheological and rheo-optical measurements. For these measurements, the solvent viscosity must be high enough. However, the high viscosity makes scattering measurements difficult, and little previous studies compared the conformation and local dynamics of polymer chains in the same solvent condition as mentioned above. Therefore, the present study makes effort to

measure small angle X-ray scattering (SAXS) on very viscous solutions to compare the results with rheological and rheo-optical results of the same solution systems.

As mentioned in the previous subsection, cellulose and amylose and their derivatives have a wide variety of the chain stiffness, so that they are suitable to study the relation between the conformation and local dynamics of polymer chains with different chain stiffness. Chapter II reports results of SAXS measurements on cellulose and amylose in the ionic liquid BmimCl and the analysis of the results by the wormlike chain model to determine λ^{-1}.

As explained in Section I-3-3, the conformation of amylose carbamate derivatives is strongly dependent on the solvent and kind of the substituent. Especially, the conformation of amylose alkyl carbamates uniquely depends on the alkyl chain length of the substituent. To reveal the conformational difference between amylose and cellulose, it may be interesting to compare the alkyl chain length dependence of the conformation of cellulose alkyl carbamates with that of amylose alkyl carbamates. The conformational studies on cellulose alkyl carbamates are described in Chapter III.

After many solubility tests, we have found that cellulose tris(phenylcarbamate) (CTPC) dissolved in tricresyl phosphate (TCP) is a suitable system to study both conformation and local chain dynamics in the same solvent condition. The conformational study on this system is reported in Chapter IV and rheological and rheo-optical studies on the same system are presented in Chapter V.

After briefly summarizing the main results and conclusions obtained in Chapters II – V, Chapter VI compares the results of the conformational study on cellulose and amylose in BmimCl presented in Chapter II with the local chain dynamics of the same systems studied by Maeda et al. The relations between the chain stiffness and local chain dynamics obtained in this work, as well as in previous studies are also summarized in Chapter VI.

References

1. S. Chandrasekhar, *Rev. Mod. Phys.* **1943,** 15, 1-89.

2. H. Yamakawa, *Modern Theory of Polymer Solutions*. Harper & Row: New York, 1971.

3. W. Kuhn, *Kolloid-Z.* **1936,** 76, 258-271.

4. W. Kuhn, *Kolloid-Z.* **1939,** 87, 3-12.

5. J. G. Kirkwood, Riseman, J. *J. Chem. Phys.* **1948,** 16, 565-573.

6. P. E., Jr. Rouse, *J. Chem. Phys.* **1953,** 21, 1272-1280.

7. B. H. Zimm, *J. Chem. Phys.* **1956,** 24, 269-278.

8. O. Kratky, G. Porod, *Recl. Trav. Chim. Pays-Bas* **1949,** 68, 1106.

9. N. Saito, K. Takahashi, Y. Yunoki, *J. Phys. Soc. Japan* **1967,** 22, 219-226.

10. H. E. Daniels, *Proc. Roy. Soc. Edinburgh, Sec. A* **1952,** 63, 290-311.

11. H. Yamakawa, T. Yoshizaki, *Helical Wormlike Chains in Polymer Solutions*. Second Edition ed.; Springer-Verlag: Berlin & Heidelberg, 2016.

12. T. Norisuye, H. Fujita, *Polym. J.* **1982,** 14, 143-147.

13. S. Amelar, C. E. Eastman, R. L. Morris, M. A. Smeltzly, T. P. Lodge, E. D. von Meerwall, *Macromolecules* **1991,** 24, 3505-3516.

14. T. Inoue, T. Uematsu, K. Osaki, *Macromolecules* **2002,** 35, 820-826.

15. E. Schweitzer, J. Prakt, *Chem.* **1857**, 72, 109.

16. R. P. Swatloski, S. K. Spear, J. D. Holbrey, R. D. Rogers, *J. Am. Chem. Soc.* **2002**, 124, 4974-4975.

17. Y. Fukaya, K. Hayashi, M. Wada, H. Ohno, *Green Chemistry*, **2008**, 10, 44-46.

18. Y. Fukaya, A. Sugimoto, H. Ohno, *Biomacromolecules*, **2006**, 7, 3295-3297.

19. N. Sun, M. Rahman, Y. Qin, M. L. Maxim, H. Rodriguez, R. D. Rogers, *Green Chemistry*, **2009**, 11, 646-655.

20. F. Schoenbein Pogg Ann **1846**, 70, 220.

21. F. J. Otto *Itzehoer Wochenblatt*; 1846, column 1626.

22. M. Kurata, W. H. Stockmayer, *Fortschr. Hochpolym.-Forsch.* **1963,** 3, 196.

23. P. J. Flory, *Makromol. Chem.* **1966,** 98, 128.

24. A. Maeda, T. Inoue, T. Sato, *Macromolecules* **2013,** 46, 7118-7124.

25. A. Maeda, Conformation and Dynamics of the Cellulose Chain in Ionic Liquids. Ph.D. Thesis, Osaka University, 2014.

26. K. Takeda, M. Shigeta, K. Aoki, H. Sasaoka, K. Sasa, H. Hirai, K. Hachiya, Y. Moriyama, *J. Colloid Interf. Sci.* **1992,** 154, 385-392.

27. Waldmann, H.; Gygax, D.; Bednarski, M. D.; Randall Shangraw, W.; Whitesides, G. M. *Carbohydrate Research* **1986,** 157, c4-c7.

28. Y. Nakanishi, T. Norisuye, A. Teramoto, S. Kitamura, *Macromolecules* **1993,** *26*, 4220-4225.

29. T. Norisuye, *Polym. J.* **1994,** *26*, 1303-1307.

30. W. Burchard, *Makromol. Chem.* **1963,** *64*, 110-125.

31. W. Burchard, Light Scattering from Polysaccharides as Soft Materials. In *Soft Matter Characterization*, Borsali, R.; Pecora, R., Eds. Springer Netherlands: 2008; pp 463-603.

32. B. Seger, T. Aberle, W. Burchard, *Carbohydrate Polymers* **1996,** 31, 105-112.

33. K. Terao, T. Fujii, M. Tsuda, S. Kitamura, T. Norisuye, *Polym. J.* **2009,** *41*, 201-207.

34. K. Terao,; F. Maeda, K. Oyamada, T. Ochiai, S. Kitamura, T. Sato, *J. Phys. Chem. B* **2012,** *116*, 12714-12720.

35. M. Tsuda, K. Terao, S. Kitamura, T. Sato, *Biopolymers* **2012,** *97*, 1010-1017.

36. K. Terao, M. Murashima, Y. Sano,; S. Arakawa, S. Kitamura, T. Norisuye, *Macromolecules* **2010,** *43*, 1061-1068.

Chapter II.

Chain Dimensions and Stiffness of Cellulosic and Amylosic Chains in an Ionic Liquid: Cellulose, Amylose, and an Amylose Carbamate in BmimCl

II-1. Introduction

Since an ionic liquid, 1-butyl-3-methylimidazolium chloride (BmimCl) was found to dissolve cellulose,[1] it has been of great interest as the solvent of polysaccharides owing to the processibility of such materials. Ionic liquids are also suitable to investigate rheological properties or polymer dynamics of polysaccharides[2-6] because they have much higher viscosity and much lower volatility than common organic solvents. The chain conformation of polysaccharides in ionic liquids is prerequisite to discuss such dynamic properties from molecular point of view. Few examples are however reported to determine chain conformation of cellulose and amylose in some ionic liquids by light scattering[7-8] because test solutions for light scattering experiments have very high viscosity, low refractive index increment, and sometimes fluorescence from the solvent.

Such experimental difficulties can be removed in small-angle X-ray scattering (SAXS). Scattered X-ray intensities were found to be high enough in for dimensional analysis in our preliminary experiments. For the similar reason, polystyrene in some viscous solvents was

investigated by small-angle neutron scattering.[9] We thus made solution SAXS measurements for cellulose, amylose, and amylose tris(ethylcarbamate) (ATEC) in BmimCl. Dissolution mechanisms of cellulose in this solvent have recently been investigated by molecular dynamics simulation.[10-12] The obtained particle scattering function data were analyzed in terms of the Kratky-Porod (KP) wormlike chain model[13] to determine the chain stiffness parameter λ^{-1} (the Kuhn segment length or twice of the persistence length). The chain stiffness parameters λ^{-1} obtained in this study for cellulose, amylose, and ATEC in BmimCl are compared with the literature results in different solvents, to argue the conformational nature of the polysaccharides in the ionic liquid.

II-2. Experimental Section

II-2-1. Samples and test solutions

II-2-1-1. Cellulose

Two cellulose samples, that is, Avicel PH-101 (Asahi Kasei) and 'Cellulose' (microcrystalline powder, Sigma) were used for this study without further purification and designated to be Cell38K and Cell37K, respectively. The weight-average molar mass M_w was estimated to be 3.8×10^4 g mol^{-1} and 3.7×10^4 g mol^{-1} for Cell38K and Cell37K, respectively, from the intrinsic viscosity $[\eta]$ in aqueous 6 wt % NaOH/4 wt % urea with the literature $[\eta]$ – M_w relationship.[14] The M_w value and the dispersity index $Đ$ defined as the ratio of M_w to the

number average molar mass were also roughly estimated for Cell38K to be $M_w = 3.6 \times 10^4$ g mol^{-1} and $Đ = 1.6$ and for Cell37K to be $M_w = 4.2 \times 10^4$ g mol^{-1} and $Đ = 1.6$, from the M_w and $Đ$ of the corresponding phenylcarbamate derivative samples which were determined from the size-exclusion chromatography with light scattering and refractive index detectors (SEC-MALS; DAWN DSP, Wyatt Technology Corp., USA) in tetrahydrofuran (THF) with the refractive index increment being 0.170 cm^{3}g^{-1}.[15] The synthesis procedure of cellulose tris(phenylcarbamate) and SEC-MALS measurements were substantially the same as those for cellulose tris(alkylcarbamate)s (see Chapter III). The slight difference in M_w may be occurred in the process of the purification of the phenylcarbamate derivative samples.

II-2-1-2. Amylose

Enzymatically synthesized two amylose samples[16] (ESA50K and ESA90K), which are the same as those recently used to synthesize amylose carbamate derivatives,[17] are chosen for this study. Their M_w values were estimated to be 5.0×10^4 g mol^{-1} and 9.3×10^4 g mol^{-1} for ESA50K and ESA90K, respectively, from $[\eta]$ in dimethylsulfoxide at 25 °C with the relationship between $[\eta]$ and M_w reported by Nakanishi et al.[18] The $Đ$ values are less than 1.2.[17]

II-2-1-3. Amylose tris(ethylcarbamate) (ATEC)

Two previously investigated ATEC samples,[19] ATEC10K and ATEC150K were used for this study. Their $Đ$ values are less than 1.1.

II-2-1-4. Solvents and preparation of test solutions

BmimCl purchased from Wako was used as a solvent of which water content was 0.9% referring to the company certificate. The solvent was dried in vacuum at 80 °C overnight. Thus, the actual water content may be smaller than the value according to the recent report for BmimCl with the similar purification (0.11 %).[20] The resultant solvent was clear with no turbidity. Each sample which was dried in vacuum at room temperature for at least 12 hours was weighed with an electronic balance in a glass bottle and an appropriate amount of solvent was added. The resultant mixtures were stored in a vacuum oven at 80-90 °C for 48 hours and then mixed with a magnetic stirrer bar for 24 hours at 60 °C to dissolve the sample. The obtained solutions were stored in a vacuum for 24 hours at 80 °C prior to the following SAXS measurements. As the preliminary solubility test for previously synthesized amylose and cellulose derivatives,[15,19,21-22] we found that amylose tris(phenylcarbamate), amylose 2-acetyl-3,6-bis(phenylcarbamate), and cellulose tris(ethylcarbamate) are soluble in BmimCl whereas cellulose tris(phenylcarbamate) is only soluble at 80 °C but the solution became turbid at room temperature. Furthermore, amylose tris(*n*-butylcarbamate), amylose tris(*n*-hexylcarbamate), and cellulose tris(*n*-butylcarbamate) are not soluble in BmimCl.

II-2-2. Small angle X-ray Scattering (SAXS) measurements

SAXS measurements were carried out for the above-mentioned solutions and the solvent at 25 °C at the BL40B2 beamline in SPring-8 (Hyogo, Japan) with the approval of the Japan Synchrotron Radiation Research Institute (JASRI) (Proposal Nos. 2014B1087, 2015A1179, 2015B1100, 2015B1674, and 2016A1053). Although this temperature is lower than the melting temperature of BmimCl, no aging effects were found in the measurement time scale in the range of temperature between −65 °C and 55 °C.[5] We note that the conformational change of cellulose should be still much quicker than the time scale even though the solvent viscosity is very high at the temperature, where it was reported to be 3.95 Pa s at 30 °C.[20] A Rigaku R-AXIS VII imaging plate was utilized to obtain two dimensional scattering intensity data. The wavelength, camera length, and accumulation time were chosen to be 0.10 nm, 4000 mm, and 300-600 s, respectively. Test solutions with several different polymer mass concentrations c ranging from 5×10^{-3} g cm^{-3} to 5×10^{-2} g cm^{-3} were measured for each polysaccharide sample in a quartz capillary cell with a diameter of 2 mmϕ. The lowest concentration for each sample was obviously lower than the overlap concentration c^* calculated from the resultant gyration radii while the highest concentration was somewhat lower or higher than c^* if we consider degradation of the cellulose sample described in the next section. It should be noted that solvent and test solutions are heated again to 80 °C to reduce the viscosity and relatively thick needles (1.2 mmϕ) were used to inject them into the capillary without air bubbles. Each

measurement was started after it was stored for 5 − 20 min at room temperature (25 °C). Scattering profiles were not affected by this aging time difference. The circular average procedure was employed to obtain angular dependence of scattering intensity $I(q)$ which has been divided by the intensity of the direct beam at the lower end of the cell to correct both the incident light intensity and the transmittance, where q denotes the magnitude of the scattering vector. The same capillary was used to measure four solutions and the solvent to determine the excess scattering intensity $\Delta I(q)$ as the difference of $I(q)$ between each solution and the solvent. We note that the $I(q)$ data for solvent were substantially independent of q in the range of $q > 0.2$ nm^{-1} and slight higher $I(q)$ was observed in the lower q range. This is likely because of stray X-ray from the light source since similar behavior was also observed for tetrahydrofuran. The Berry square-root plot[23] was utilized to extrapolate the scattering intensity to infinite dilution to determine the z-average mean square radius of gyration $\langle S^2 \rangle_z$ and the particle scattering function $P(q)$.

II-3. Results and Discussion

Figure II-1 illustrates the Berry plots of $[c/\Delta I(q)]^{1/2}$ vs q^2 for Cell38K and ESA50K in BmimCl both at 25 °C. Dashed lines in the figure indicate the initial slope to determine $\langle S^2 \rangle_z$ and $P(q)$. The second virial coefficient A_2 was estimated from the slope of $[c/\Delta I(0)]^{1/2}$ (filled squares) using the M_w data mentioned in the former section with the same method reported in

ref 42, in which the optical constant was estimated from $[c/\Delta I(0)]_{c=0}^{1/2}$ and the M_w value. The resultant $\langle S^2 \rangle_z$ and A_2 data are listed in Table II-1 along with the M_w values. The latter value (A_2) are between 4×10^{-5} and 3.5×10^{-4} mol cm^3g^{-2}, indicating that all the polymer-solvent systems investigated in this study are good solvent systems. Actual values of M_w and A_2 for cellulose (and amylose) in BmimCl may be smaller and larger than these values, respectively, owing to the degradation during the dissolution process as we mention later.

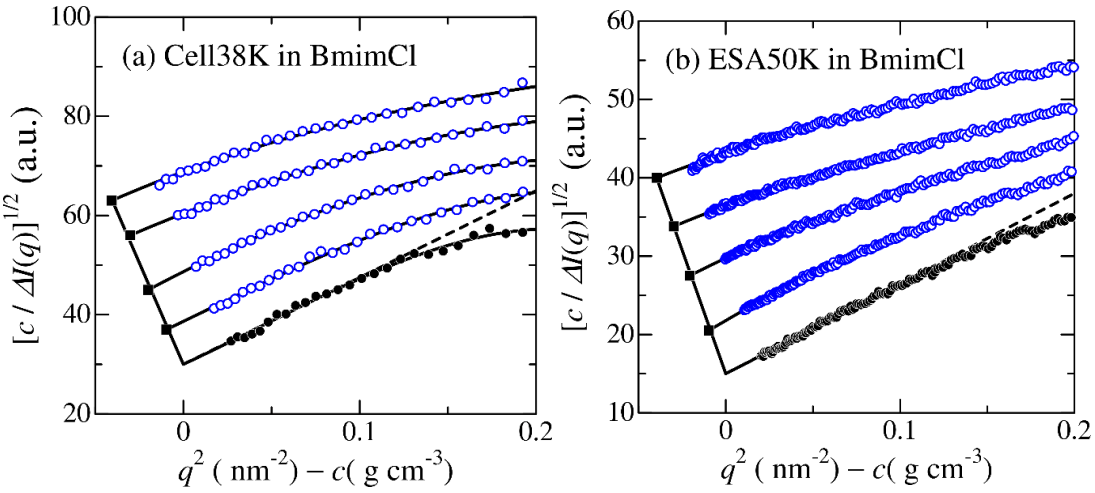

Figure II-1. Square root Zimm plots (Berry plots) for Cell38K (a) and ESA50K (b) in BmimCl at 25 °C. Filled circles and squares show extrapolated values to $c = 0$ and $q^2 = 0$, respectively.

Table II-1. Molecular Characteristics of Cellulose, Amylose, and ATEC samples in BmimCl at 25 ˚C

Samples	M_w (10^4 g mol^{-1})	$\langle S^2\rangle_z^{1/2}$ (nm)	$\langle S^2\rangle_{calc}^{1/2}$ (nm) [b]	A_2 (10^{-4} mol cm^3 g^{-2})
Cell37K	3.7	7.1	7.7 [c]	3.5 [d]
Cell38K	3.8	5.7	6.4 [c]	3.2 [d]
ESA50K	5.0	6.6	7.0	3.3 [d]
ESA90k	9.3	7.6	8.2	1.8 [d]
ATEC10K	1.02 [a]	2.7	2.1	1.5
ATEC150K	15.4 [a]	11.7	12.0	0.4

[a] Ref 17. [b] Calculated values for the KP wormlike chain with the parameters in Table II-2. [c] z-average value with $Đ$ = 1.6. [d] Assuming no degradation in the dissolution process.

The obtained $P(q)$ data are displayed in the form of the reduced Holtzer plot in Figure II-2. The shape for almost all samples are typical for wormlike chains, namely, a flat plateau is found for each sample in high q range with an appreciable peak at low q except for ATEC10K. The particle scattering function $P(q)$ for the touched-bead wormlike chain is expressed as[25-26]

$$P(q) = 9\left(\frac{2}{qd}\right)^6\left(\sin\frac{qd}{2} - \frac{qd}{2}\cos\frac{qd}{2}\right)^2 P_0(q) \qquad \text{(II-1)}$$

where $P_0(q)$ is the particle scattering function for the thin wormlike chain as follows.

$$P_0(q) = \frac{2}{L^2}\int_0^L (L-t)\, I\left(\lambda^{-1}q;\lambda t\right) dt \qquad \text{(II-2)}$$

Here L, d, and $I(\lambda^{-1}q; \lambda t)$ are the contour length, the bead diameter, and the characteristic function of the KP chain which can be calculated by means of the approximate expression by Nakamura and Norisuye.[27-28] A curve fitting procedure was carried out for each sample to determine the three parameters, λ^{-1}, L, and d. Nicely fitted theoretical curves in Figure II-2 indicate that the KP chain is a good model to explain the current $P(q)$ data. The three parameters summarized in Table II-2 were unequivocally determined for almost all samples other than ATEC10K for which λ^{-1} was assigned the value obtained for the higher M_w sample, ATEC150K. Very small d values may be reasonable because this parameter reflects the electron density profiles of the chain cross section. Indeed, such small d was also found for other polymer-solvent systems[29-30] and it can be explained by some appropriate models such as the concentric double cylinder as described in Chapter III. We considered molar mass distribution for cellulose samples assuming log-normal distribution because their $Đ$ values (1.6) are somewhat larger than those for the other samples (1.1 – 1.2). The resultant theoretical values (red curves) slightly better fit the experimental data than the monodisperse case (blue curves).

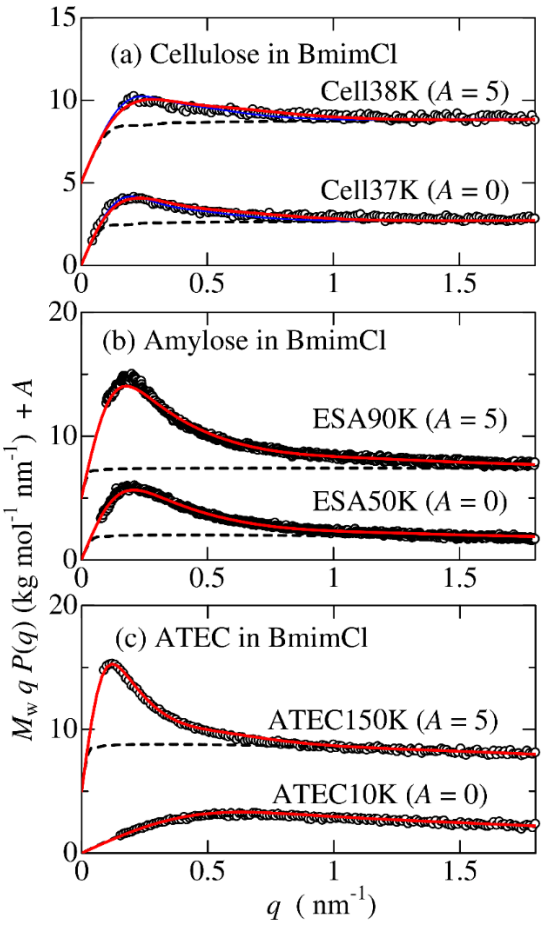

Figure II-2. Reduced Holtzer plots for (a) cellulose in BmimCl, (b) amylose in BmimCl, and (c) ATEC in BmimCl at 25 °C. Solid and dashed curves indicate the theoretical values for the touched bead wormlike chain and the touched bead rigid rod, respectively. Red and blue curves in panel (a) correspond to $Đ = 1.6$ and $Đ = 1$, respectively.

Table II-2. Wormlike Chain Parameters for Cellulose, Amylose, and ATEC samples in BmimCl at 25 ˚C.

sample	L (nm)	λ^{-1} (nm)	d (nm)
Cell37K	43 ± 3	7 ± 1 (9 ± 1)[b]	0
Cell38K	31 ± 2	7 ± 1 (9 ± 1)[b]	0
ESA50K	90 ± 15	3.5 ± 0.5	0
ESA90K	115 ± 15	3.7 ± 0.5	0
ATEC10K	9.0 ± 0.5	7.5 [a]	1.5 ± 0.1
ATEC150K	125 ± 10	7.5 ± 0.5	1.3 ± 0.1

[a] Assumed. [b] Parameter with $Đ = 1$.

The radius of gyration $\langle S^2 \rangle_{calc}$ for the KP wormlike chain is calculated from the following Benoit-Doty equation [31]

$$\left\langle S^2 \right\rangle = \frac{L}{6\lambda} - \frac{1}{4\lambda^2} + \frac{1}{4\lambda^3 L} - \frac{1}{8\lambda^4 L^2}\left[1 - \exp\left(-2\lambda L\right)\right] \qquad \text{(II-3)}$$

for each sample with the parameters listed in Table II-2. The resultant values are substantially close to that for the experimental values, indicating the obtained wormlike chain parameters consistently explain both $P(q)$ and $\langle S^2 \rangle_z$. Since the Kuhn segment number defined as λL for all samples are in the range from 1.2 to 31, the intramolecular excluded-volume effects may be negligible.[32-34] Twice larger λ^{-1} value estimated for cellulose in 1-allyl-3-methylimidazolium chloride (AmimCl) in the previous report[7] is likely due to the excluded volume effect as well

as the molar mass distribution. Indeed, the Kuhn segment number was roughly estimated for their sample to be 180 with λ^{-1} = 7 nm and the helix pitch per residue h = 0.515 nm. It is also noted that the local helical structure of amylose is rather unimportant for the current q range while it becomes more dominant for lower molar mass amylose at higher q range.[35] Thus, we do not show further analysis in terms of the helical wormlike chain model although this model is rather better to explain the viscosity behavior in dimethylsulfoxide.[18]

If we calculate h from L in Table II-2 defined as $h = LM_0 / M_w$ with M_0 being molar mass per repeat unit, the h value is estimated as 0.19 and 0.13 nm for Cell37K and Cell38K, respectively. These are much smaller than those for cellulose in solution[14, 36-37] (0.45 – 0.51 nm), cellulose derivatives in solution (0.40 – 0.51 nm, see Chapter III), and cellulose molecules in crystal[38] (0.52 nm). This extremely small h values for cellulose in BmimCl suggest that degradation of cellulose molecules in the process of dissolution as depicted by some other researchers.[39-40] It is however noted that this degradation may not affect the determination of λ^{-1} unless $Đ$ does not change significantly. While ESA50K has relatively reasonable h value of 0.29 nm, which is close to that for amylose in solution 0.33 nm,[18] ESA90K has smaller h value of 0.20 nm. Degradation of amylose in the dissolution process is thus less likely than it is for cellulose. The main chain hydrolysis by solvent ionic liquid may become less prominent for polysaccharide derivatives. Indeed, the h value estimated for ATEC10K and

ATEC150K to be 0.32 and 0.29 nm are not very different from those reported in other solvents, 0.35 – 0.38 nm.[19]

The obtained chain stiffness parameters for the three polymers in BmimCl are summarized in Table II-3 with the literature values in various solvents. The following is the discussion for each system.

II-3-1. Cellulose in BmimCl

Although cellulose is not soluble in common organic and inorganic solvents owing to the intramolecular hydrogen bonding, several kinds of aqueous alkaline solutions containing metal complexes were developed. Representative Kuhn segment lengths reported in last two decades are listed in Table II-3.[8, 14, 36, 41-44] The currently obtained λ^{-1} value in BmimCl is the smallest of the solvent systems. Conformational energy calculations[45-47] demonstrated that the cellulosic chain takes an extended conformation with λ^{-1} as large as 60 nm, but if the bond angle of the glucosidic bridge slightly increases from that in the crystalline state, a new energetically stable rotational state appears which acts as a kink and remarkably reduces λ^{-1}.[47] The experimental values of λ^{-1} in Table II-3 are much smaller than 60 nm, which may be explained by the quasi-stable (kink) conformation as well as the underestimated torsion angle fluctuation. According to the modern molecular dynamics for an oligo cellulose, intramolecular hydrogen bonds of cellulose disrupted in BmimCl.[10, 12] Similar reduction of

intramolecular hydrogen bonds was also reported in other ionic liquids.[48] Smaller λ^{-1} for cellulose in BmimCl than in aqueous 6 wt % NaOH/4 wt % urea is most likely due to the decrease of intramolecular hydrogen bonds since such hydrogen bonds may remain in the latter solvent.[49]

II-3-2. Amylose in BmimCl

Native amylose extracted from starch has some branching structure.[50-51] We thus compared λ^{-1} data for enzymatically synthesized amylose (ESA) in dimethylsulfoxide (DMSO) and a metal complex. Conformational energy calculations for amylose[35, 52-55] give us a single broad minimum in the conformational energy map, which provides 0.8 – 4 nm for λ^{-1} of which the value depends on the force field.[35] The estimated λ^{-1} range from the simulation includes the experimental results in BmimCl, as well as common organic solvents and aqueous solutions reported. The λ^{-1} value in FeTNa is much larger than these values. This is likely because carboxy groups of tartrate may form hydrogen bonds with hydroxy groups of amylose, which may severely restrict the fluctuation of the internal rotation about the glucosidic linkage.

II-3-3. ATEC in BmimCl

The fraction of the intramolecular hydrogen bonding C=O and N-H groups determines the chain stiffness of amylose alkylcarbamate derivatives, so that λ^{-1} depends significantly on the

hydrogen-bonding ability of the solvent.[19, 22, 56] Methanol is an intramolecular hydrogen-bonding breaking solvent for the amylose derivatives, and infrared (IR) absorption demonstrated almost no intramolecular hydrogen bonds of ATEC in methanol.[19] The chain stiffness in BmimCl is close or slightly smaller than that in methanol. It is thus concluded that the flexibility of the ATEC chain in BmimCl comes from the breakage of the intramolecular hydrogen bonds of ATEC although IR absorption by BmimCl makes difficult to check the fraction of the intramolecular hydrogen bonding by IR spectroscopy.

Table II-3. Kuhn Segment Length λ^{-1} for Cellulose, Amylose, and ATEC in Various Solvents.

polymer	solvent	λ^{-1} (nm)	Reference
cellulose	1-butyl-3-methylimidazolium chloride (BmimCl)	7 ± 1	this work
	aqueous $Cd(en)_3(OH)_2$ (cadoxen)	8	8, 56
	0.5 M aqueous $Cu(en)_3(OH)_2$ (en = ethylenediamine)	9	42
	aqueous $Ni(tren)(OH)_2$ [tren = tris(2-aminoethyl)amine]	10	36
	4.6 wt % LiOH/15 wt % urea in water	12	43
	6 wt % NaOH/4 wt % urea in water	12	14
	aqueous $Cu(NH_3)_4(OH)_2$ (cuoxam)	13	36
	aqueous $Cd(tren)(OH)_2$	16	36
	DMAc with 0.5% LiCl	16	42
	1,3-dimethyl-2-imidazolidinone (DMI) with 1% LiCl	18	44
	dimethylacetoamide (DMAc) with 8% LiCl	18	44
	aqueous iron-sodiumtartrate (FeTNa)	21	41
amylose (ESA)	BmimCl	3.5 ± 0.5	this work
	dimethylsulfoxide (DMSO)	2.4 (4)[a]	18
	DMSO with 43.5 vol % acetone	2.4 (4)[a]	57-58
	formamide	2.4 (4)[a]	57-58
	0.5 M aqueous NaOH	2.4 (4)[a]	57-58
	water	2.4 (4)[a]	57-58
	aqueous FeTNa	18	41
ATEC	BmimCl	7.5 ± 0.5	this work
	methanol	9	19
	2-methoxyethanol	14	19
	L-ethyl lactate	15	19
	D-ethyl lactate	27	19
	tetrahydrofuran (THF)	33	20

[a] For the helical wormlike chain.

II-4. Conclusion

The chain stiffness parameter λ^{-1} was successfully determined for cellulose, enzymatically synthesized amylose (ESA), and amylose tris(ethylcarbamate) (ATEC) in an ionic liquid (BmimCl). While some chain degradation was observed especially for cellulose, clear scattering data were obtained for all systems. Analyses in terms of the wormlike chain shows that all the three polymers have rather flexible main chain in BmimCl while cellulose and ATEC behave as semiflexible or stiff chains in other solvents. This is most likely due to disrupt intramolecular hydrogen bonds and/or to increase conformational fluctuation around the most stable conformation.

References

1. R. P. Swatloski, S. K. Spear, J. D. Holbrey, R. D. Rogers, *J. Am. Chem. Soc.* **2002,** *124*, 4974-5.

2. Q. L. Kuang, J. C. Zhao, Y. H. Niu, J. Zhang, Z. G. Wang, *J. Phys Chem B* **2008,** *112*, 10234-40.

3. J. Horinaka, R. Yasuda, T. Takigawa, *J. Polym. Sci., Part. B: Polym. Phys.* **2011,** *49*, 961-965.

4. X. Chen, Y. M. Zhang, H. P. Wang, S. W. Wang, S. W. Liang, R. H. Colby, *J. Rheol.* **2011,** *55*, 485-494.

5. A. Maeda, T. Inoue, T. Sato, *Macromolecules* **2013,** *46*, 7118-7124.

6. Y. Ahn, S. Y. Kwak, Y. Song, H. Kim, *Physical chemistry chemical physics : PCCP* **2016,** *18*, 1460-9.

7. Y. Chen, Y. M. Zhang, F. Y. Ke, J. H. Zhou, H. P. Wang, D. H. Liang, *Polymer* **2011,** *52*, 481-488.

8. A. Maeda, Conformation and Dynamics of the Cellulose Chain in Ionic Liquids. Ph.D. Thesis, Osaka University, 2014.

9. T. P. Lodge, K. C. Hermann, M. R. Landry, *Macromolecules* **1986,** *19*, 1996-2002.

10. H. Xu, W. Pan, R. Wang, D. Zhang, C. Liu, *J. Comput. Aided Mol. Des.* **2012,** *26*, 329-37.

11. A. S. Gross,; A. T. Bell,; J. W. Chu, *Physical chemistry chemical physics : PCCP* **2012,** *14*, 8425-30.

12. B. Mostofian, X. Cheng, J. C. Smith, *J Phys Chem B* **2014,** *118*, 11037-49.

13. O. Kratky, G. Porod, *Recl. Trav. Chim. Pays-Bas* **1949,** *68*, 1106-1122.

14. J. P. Zhou, L. N. Zhang, J. Cai, *J. Polym. Sci., Part. B: Polym. Phys.* **2004,** *42*, 347-353.

15. F. Kasabo, T. Kanematsu, T. Nakagawa, T. Sato, A. Teramoto, *Macromolecules* **2000,** *33*, 2748-2756.

16. S. Kitamura, H. Yunokawa, S. Mitsuie, T. Kuge, *Polym. J.* **1982,** *14*, 93-99.

17. K. Terao, T. Fujii, M. Tsuda, S. Kitamura, T. Norisuye, *Polym. J.* **2009,** *41*, 201-207.

18. Y. Nakanishi, T. Norisuye, A. Teramoto, S. Kitamura, *Macromolecules* **1993,** *26*, 4220-4225.

19. K. Terao,; F. Maeda, K. Oyamada, T. Ochiai, S. Kitamura, T. Sato, *J. Phys. Chem. B* **2012,** *116*, 12714-12720.

20. Q. Kuang, J. Zhang, Z. Wang, *J Phys Chem B* **2007,** *111*, 9858-63.

21. M. Tsuda, K. Terao, S. Kitamura, T. Sato, *Biopolymers* **2012,** *97*, 1010-1017.

22. K. Terao, M. Murashima, Y. Sano,; S. Arakawa, S. Kitamura, T. Norisuye, *Macromolecules* **2010,** *43*, 1061-1068.

23. G. C. Berry, *J. Chem. Phys.* **1966,** *44*, 4550-4564.

24. Y. Jiang, X. Zhang, B. Miao, D. Yan, *J. Chem. Phys.* **2015,** *142*, 154901.

25. K. Nagasaka, T. Yoshizaki, J. Shimada, H. Yamakawa, *Macromolecules* **1991,** *24*, 924-931.

26. W. Burchard, K. Kajiwara, *Proc. R. Soc. London, Ser. A* **1970,** *316*, 185-199.

27. Y. Nakamura, T. Norisuye, *J. Polym. Sci., Part. B: Polym. Phys.* **2004,** *42*, 1398-1407.

28. Y. Nakamura, T. Norisuye, Brush-Like Polymers. In *Soft Matter Characterization*, Borsali, R.; Pecora, R., Eds. Springer Netherlands: 2008; pp 235-286.

29. S. Arakawa, K. Terao, S. Kitamura, T. Sato, *Polym. Chem.* **2012,** *3*, 472-478.

30. Y. Nagata, H. Hasegawa, K. Terao, M. Suginome, *Macromolecules* **2015,** *48*, 7983-7989.

31. H. Benoit, P. Doty, *J. Phys. Chem.* **1953**, 57, 958-963.

32. H. Yamakawa, T. Yoshizaki, *Helical Wormlike Chains in Polymer Solutions, 2nd ed.* Springer: Berlin, Germany, 2016.

33. T. Norisuye, H. Fujita, *Polym. J.* **1982,** *14*, 143-147.

34. T. Norisuye, A. Tsuboi, A. Teramoto, *Polym. J.* **1996,** *28*, 357-361.

35. J. Shimada, H. Kaneko, T. Takada, S. Kitamura, K. Kajiwara, *J. Phys. Chem. B* **2000,** *104*, 2136-2147.

36. K. Saalwachter, W. Burchard, P. Klufers, G. Kettenbach, P. Mayer, D. Klemm, S. Dugarmaa, *Macromolecules* **2000,** *33*, 4094-4107.

37. J. Cai, Y. T. Liu, L. N. Zhang, *J. Polym. Sci., Part. B: Polym. Phys.* **2006,** *44*, 3093-3101.

38. Y. Nishiyama, P. Langan, H. Chanzy, *J. Am. Chem. Soc.* **2002,** *124*, 9074-9082.

39. O. M. Gazit, A. Katz, *ChemSusChem* **2012,** *5*, 1542-8.

40. H. Zhang, J. Wu, J. Zhang, J. S. He, *Macromolecules* **2005,** *38*, 8272-8277.

41. B. Seger, T. Aberle, W. Burchard, *Carbohydr. Polym.* **1996,** *31*, 105-112.

42. M. Kes, B. E. Christensen, *J. Chromatogr. A* **2013,** *1281*, 32-7.

43. J. Cai, Y. T. Liu, L. N. Zhang, *J. Polym. Sci., Part. B: Polym. Phys.* **2006,** *44*, 3093-3101.

44. M. Yanagisawa, A. Isogai, *Biomacromolecules* **2005,** *6*, 1258-65.

45. N. Yathindra,; V. S. R. Rao, Cellulose. *Biopolymers* **1970,** *9*, 783-790.

46. K. D. Goebel, C. E. Harvie, D. A. Brant, *Appl. Polym. Symp.* **1976,** *28*, 671-691.

47. H. Yanai, T. Sato, *Polym. J.* **2006,** *38*, 226-233.

48. R. S. Payal, S. Balasubramanian, *Physical chemistry chemical physics : PCCP* **2014,** *16*, 17458-65.

49. Z. Jiang, Y. Fang, J. Xiang, Y. Ma, A. Lu, H. Kang, Y. Huang, H. Guo, R. Liu, L. Zhang, *J. Phys. Chem. B* **2014,** *118*, 10250-7.

50. Y. Takeda, N. Maruta, S. Hizukuri, *Carbohydr. Res.* **1992,** *227*, 113-120.

51. Y. Takeda, S. Tomooka, S. Hizukuri, *Carbohydr. Res.* **1993,** *246*, 267-272.

52. C. V. Goebel, D. Brant, W. Dimpfl, *Macromolecules* **1970,** *3*, 644-654.

53. D. Brant, W. Dimpfl, *Macromolecules* **1970,** *3*, 655-664.

54. R. C. Jordan, D. A. Brant, A. Cesàro, *Biopolymers* **1978,** *17*, 2617-2632.

55. Y. Nakata, S. Kitamura, K. Takeo, T. Norisuye, *Polym. J.* **1994,** *26*, 1085-1089.

56. D. Henley, *Arkiv for Kemi* **1961,** *18*, 327-392.

57. T. Norisuye, *Polym. J.* **1994,** *26*, 1303-1307.

58. W. Burchard, 24. *Makromol. Chem.* **1963,** *64*, 110-125.

Chapter III.

Dimensional and Hydrodynamic Properties of Cellulose Tris(alkylcarbamate)s in Solution: Side Chain Dependent Conformation in Tetrahydrofuran

III-1. Introduction

Cellulose tris(phenylcarbamate) (CTPC) was originally utilized to elucidate the conformational properties of cellulose (β-1,4-glucan) because hydroxyl groups of cellulose tend to form intermolecular hydrogen bonds with other cellulose molecules.[1] Dimensional and hydrodynamic properties of CTPC[2-7] can be explained by the Kratky-Porod wormlike chain model.[8] Consequently, it behaves as a typical semiflexible polymer in solution. According to the latest investigation of CTPC, the chain stiffness parameter λ^{-1} of the model (the Kuhn segment length or twice of the persistence length) was determined as 21 nm in tetrahydrofuran (THF)[6] and 16 nm in 1-methyl-2-pyrrolidone (NMP).[9] Similar chain stiffness was also reported to be 16 nm in NMP for cellulose tris(3,5-dimethylphenylcarbamate)[10, 11] which is widely used for chiral stationary phase for liquid chromatography.[12, 13] These values are rather similar to those for cellulose, that is, λ^{-1} = 10-50 nm depending on solvents,[14-23] cellulose myristate (λ^{-1} = 23 nm),[24] and (cyanoethyl)(hydroxypropyl)cellulose (λ^{-1} = 29 nm).[25]

We recently found that some derivatives of amylose (α-1,4-glucan) have significant side chain dependent chain conformation. For example, amylose tris(*n*-butylcarbamate) (ATBC) and amylose tris(*n*-hexylcarbamate) (ATHC) form tightly wounded helical structure in THF with very high chain stiffness (λ^{-1} = 75 nm) stabilized by the intramolecular hydrogen bonding between NH and C=O groups of the neighboring repeat units.[26, 27] This value is indeed about 20 times larger than that for amylose in dimethyl sulfoxide (λ^{-1} = 4 nm)[28] and 3.6 times larger

than that for amylose tris(phenylcarbamate) in 1,4-dioxane (λ^{-1} = 21 nm).[29] On the contrary, amylose tris(ethylcarbamate) (ATEC) has appreciably smaller λ^{-1} (= 33 nm) in THF, suggesting that the intramolecular interactions between main chain and alkyl side groups play an important role for the main chain conformation of polysaccharide derivatives.[27] These results imply us to investigate cellulose alkylcarbamates since no dimensional and hydrodynamic data are available in our knowledge.

We thus synthesized three cellulose alkylcarbamates, that is, cellulose tris(ethylcarbamate) (CTEC), cellulose tris(*n*-butylcarbamate) (CTBC), and cellulose tris(*n*-octadecylcarbamate) (CTODC) of which chemical structures are shown in Figure III-1; note that CTEC and CTBC were originally synthesized by MacCormick et al.[30] and Schurig et al.,[31] respectively. Dimensional and hydrodynamic properties in THF were studied to determine the wormlike chain parameters and furthermore to elucidate how alkyl carbamate groups affect the conformational properties of cellulose derivatives.

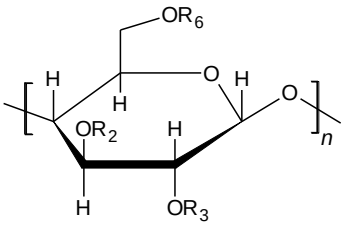

1. $R_2 = R_3 = R_6 = CONHC_2H_5$
2. $R_2 = R_3 = R_6 = CONHC_4H_9$
3. $R_2 = R_3 = R_6 = CONHC_{18}H_{37}$

Figure III-1. Chemical structures of cellulose tris(ethylcarbamate) (1. CTEC), cellulose tris(*n*-butylcarbamate) (2. CTBC), and cellulose tris(*n*-octadecylcarbamate) (3. CTODC).

III-2. Experimental Procedures

III-2-1. Preparation of Samples and Their Solutions

CTEC, CTBC, and CTODC samples were synthesized from commercially available cellulose powder (Wako, Japan) and micro crystalline cellulose (Sigma-Aldrich, USA) with an excess amount of corresponding isocyanate (ethylisocyanate, *n*-butylisocyanate, or *n*-octadecylisocyanate) in a manner similar to that reported previously for cellulose[30] and amylose.[26, 27, 32] A typical procedure for a CTBC sample is as follows.

Cellulose (4 g, 0.025 mol) and LiCl (4 g) dried in vacuum at 80 °C for several hours were dissolved in *N*,*N*-dimethylacetamide (40 cm^3) at 120 °C under argon atmosphere for 12 h. Distilled pyridine (100 cm^3) and an excess amount of *n*-butylisocyanate (22 g, 0.22 mol) were added to the mixture for 12 h at 120 °C under argon atmosphere and stirred by magnetic bar to achieve complete reaction. After the reaction, the mixture became a clear brown solution. The product was poured into a large amount of water to precipitate the crude CTBC sample. After drying in vacuum, a colorless fibrous sample was obtained. In the case of CTODC, twice amount of toluene was added to the reaction mixture to avoid gelation after adding the corresponding isocyanate. We have also attempted to prepare cellulose tris(*n*-hexylcarbamate) (CTHC) samples with *n*-hexylisocyanate because dilute solution properties of ATHC were reported.[27] We did not however use the CTHC samples in the following study because the crude product was not soluble in THF. *N*,*N*-dimethylacetamide (dehydrated grade, Wako), LiCl (Wako), ethylisocyanate (Wako), *n*-butylisocyanate (Wako), and *n*-octadecylisocyanate (Wako) were used without further purification while pyridine and toluene was purified by fractional distillation over CaH_2.

The synthesized CTEC and CTBC samples were divided into several fractions by fractional precipitation with THF as solvent and water as precipitant. Similar procedure was also employed for CTODC with THF as solvent and methanol or acetone as precipitants.

Appropriate middle fractions summarized in Table III-2 as well as the unfractionated CTEC (CTEC-U) and CTBC (CTBC-U) samples were chosen for this study. Their chemical structures were confirmed by solution ^{1}H NMR spectra in $CDCl_3$, IR absorption spectra, and elemental analysis. The weight ratio of nitrogen to carbon for each sample is consistent with the theoretical value within 2%. The degree of substitution (DS) of CTEC and CTBC samples were estimated to be 3.0 ± 0.3 from the ratio. The reprecipitated samples were dried in vacuum for more than 48 hours prior to preparation of THF solution. The solvent THF was distilled over CaH_2 except for the mobile phase of the size exclusion chromatography (SEC).

Solubility test of the CTEC, CTBC, and CTODC samples into various organic solvents was also performed to compare it with the corresponding amylose derivatives as summarized in Table III-1. While CTBC, ATBC,[26, 33] and ATEC[27] are soluble in various alcohols, CTEC has much less solubility in them other than methanol. This suggests that difference in the main chain linkage (α or β) significantly effects the solubility as is the case with the difference in cellulose and amylose. In the case of CTODC, the long side groups decrease the solubility into polar solvents while that in THF is good enough to determine dilute solution properties as discussed later.

Table III-1. Solubility of Cellulose and Amylose Alkylcarabamates in Organic Solvents at Room Temperature.

solvent	CTEC	ATEC [a]	CTBC	ATBC [b]	ATHC [a]	CTODC
chloroform	S	S	S	S	S	S
THF	S	S	S	S	S	S
methanol	S	S	S	S	I	I
2-propanol	I	S	S	S	I	I
1-propanol	I	S	S	S	S	I
2-butanol	I	S	S	S	S	I
1-butanol	I	S	S	S	S	I
2-ethoxyethanol	I	S	S	S	I	I

S: soluble. I: insoluble. ATEC: amylose tris(ethylcarbamate). ATBC: amylose tris(*n*-butylcarbamate). ATHC: amylose tris(*n*-hexylcarbamate). [a] Refs 27. [b] Refs 26, 33.

III-2-2. Size Exclusion Chromatography with Multi-angle Light Scattering (SEC-MALS)

SEC-MALS measurements were made for the CTEC, CTBC, and CTODC samples to determine their weight-average molar mass M_w and the *z*-average mean-square radius of gyration $\langle S^2 \rangle_z$ as a function of the elution volume V_e (Figure III-2). A TSKguardcolumn H_{XL}-H column and a TSKgel H_{XL} column are connected in series, and a sample loop with 100 μL was used, and the flow rate was set to be 0.5 mL min^{-1}. Mass concentration *c* of the injected solution were chosen to be $2 \times 10^{-3} - 6 \times 10^{-3}$ g cm^{-3}. A DAWN DSP multi-angle light scattering photometer and a refractive index detector were used to determine the Rayleigh ratio and *c* at each V_e, respectively. The refractive index increment $\partial n/\partial c$ values at which the wavelength of the light scattering photometer (λ_0 = 633 nm) in THF at 25 °C were determined to be 0.0841 cm^3 g^{-1} for CTEC, 0.0872 cm^3 g^{-1} for CTBC, and 0.0770 cm^3 g^{-1} for CTODC.

The scattering data were extrapolated to infinite dilution and to zero angle with the aid of the Berry plot[34, 35] and the second virial coefficients determined by SAXS measurements for each system. The obtained M_w and the dispersity index $Đ$ ($\equiv M_w / M_n$) for each sample except for the unfractionated samples (CTEC-U and CTBC-U) are shown in Table III-2. These M_w values were at most 1 % larger than the uncorrected data at finite concentration.

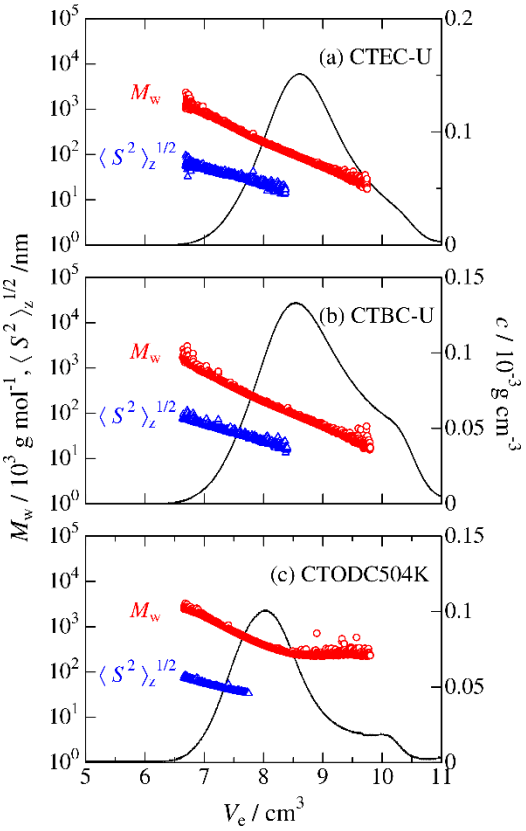

Figure III-2. Elution volume V_e dependence of the weight-average molar mass M_w (red circles), the *z*-average mean-square radius of gyration $\langle S^2 \rangle_z^{1/2}$ (blue triangles), and the polymer mass concentration c (solid curves) for (a) CTEC-U and (b) CTBC-U, and (c) CTODC504K in THF.

III-2-3. Small-Angle X-ray Scattering (SAXS)

SAXS measurements were carried out for CTEC83K, CTEC68K, CTEC43K, CTBC64K, CTBC18K, CTODC89K, and CTODC35K in THF at 25 °C at the BL40B2 beamline in SPring-

8 (Hyogo, Japan) with the approval of the Japan Synchrotron Radiation Research Institute (JASRI) (Proposal Nos. 2015B1100, 2016A1053, and 2016B1088). Test solutions with four different concentrations ranging from 4×10^{-3} to 2×10^{-2} g cm^{-3} were prepared for each sample. Solvent and solutions having different c were measured in a quartz glass capillary with a diameter of 2.0 mm. It should be noted that some preliminary measurements were also performed at the BL6A beamline in KEK-PF to estimate the measurement conditions (not shown in this paper) under the approval of the Photon Factory Program Advisory Committee (No. 2015G543). The wavelength, camera length, and accumulation time were set to be 0.10 nm, 4000 mm, and 120-300 s. Two dimensional scattering intensity data were recorded by a RIGAKU R-AXIS VII imaging plate. The actual camera length was determined by means of the Bragg reflection of silver behenate. The circular average was utilized to obtain scattering intensity $I(q)$ as a function of the magnitude of the scattering vector q. The background was measured from the scattering intensity of pure solvent in the exactly the same cell to determine the excess scattering intensity $\Delta I(q)$. The scattering intensities for each solution or solvent were corrected for the incident-beam intensity and the transmittance, both determined using ion chambers installed at the upper and lower ends of the capillary. The Berry square-root plots[34] were utilized to determine $\langle S^2 \rangle_z$ and the particle scattering function $P(q)$. The second virial coefficients A_2 were also estimated from the concentration dependence with the method as reported elsewhere.[36]

III-2-4. Viscometry

Solvent and solution viscosities for the CTEC43K, CTEC68K, CTEC83K, CTEC140K, CTBC64K, CTBC190K, CTBC254K, CTODC89K, CTODC346K, and CTODC504K in THF at 25 °C were measured using a Ubbelohde-type viscometer. The intrinsic viscosity $[\eta]$ and the Huggins constant k' were determined from the Huggins, Fuoss-Mead, and Billmeyer plots.

The resultant k' values were between 0.43 and 0.50 for CTEC, between 0.41 and 0.53 for CTBC and, between 0.36 and 0.42 for CTODC, suggesting that THF is a good solvent for the three cellulose derivatives.

III-2-5. Infrared (IR) Absorption

IR absorption measurements were made for CTEC43K, CTBC190K and CTODC346K in THF at 25 °C on an FT/IR-4200 (JASCO) spectrometer with a solution cell made of CaF_2 having 0.05 mm path length. Concentrations of the test solutions were set to be 0.02 g cm^{-3}.

III-3. Results

III-3-1. Experimental Results of the Dimensional and Hydrodynamic pProperties in THF

Figure III-3 illustrates q^2 dependence of $P(q)^{-1/2}$ for CTEC, CTBC, and CTODC samples in THF at 25 °C at low-q range. The $\langle S^2 \rangle_z^{1/2}$ values were determined from the initial slope and listed in Table III-2, along with $[\eta]$. The average A_2 values for relatively low molar mass CTEC, CTBC and CTODC were estimated from SAXS data to be 1×10^{-4}, 3×10^{-4}, and 2×10^{-4} cm^3 mol g^{-2}, indicating that THF is a good solvent for the three cellulose carbamates as in the case of k'.

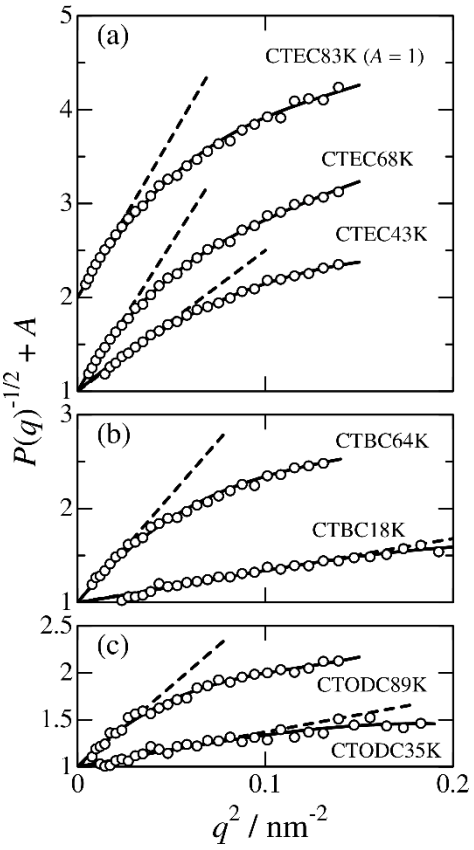

Figure III-3. Berry plots for indicated (a) CTEC, (b) CTBC, and (c) CTODC samples in THF at 25 °C. The ordinate values for CTEC83K are shifted by *A*. Dashed lines indicate the initial slopes to determine $\langle S^2 \rangle_z$.

Table III-2. Molecular Characteristics and Physical Properties of CTEC, CTBC, and CTODC Samples in THF at 25 °C.

Sample	M_w /10^3 g mol^{-1}	$Đ$ [a]	DS	$\langle S^2 \rangle_z^{1/2}$ / nm	$[\eta]$ / cm^{3}g^{-1}
CTEC43K	43.3	1.5	3.0	9.49	46.0
CTEC68K	68.2	1.2	3.2	13.2	70.0
CTEC83K	82.5	1.6	3.3	14.3	75.0
CTEC140K	140	1.6	3.2	-	111
CTBC18K	17.8	1.3	3.2	4.52	
CTBC64K	64.4	2.1	3.3	11.7	59.0
CTBC190K	190	1.3	3.3	-	132
CTBC254K	254	1.3	3.2	-	197
CTODC35K	34.7	1.3	-	4.71	
CTODC89K	88.9	1.4	-	10.2	30.5
CTODC346K	346	1.3	-	-	99.0
CTODC504K	504	1.4	-	-	110

[a] Defined as M_w / M_n

Molar mass dependence of $\langle S^2\rangle_z^{1/2}$ is displayed in Figure III-4 for CTEC, CTBC and CTODC in THF at 25 °C. The slope at lower M_w range for the three cellulose derivatives are 0.75, 0.78, and 0.82, and they decrease with increasing M_w. These are typical behavior for semirigid polymer chains in solution. Figure III-5 shows the experimental [η] data plotted against M_w for the three cellulose carbamates in THF. Their slopes are 0.81, 0.81, and 0.79 for CTEC, CTBC and CTODC, supporting the results from $\langle S^2\rangle_z^{1/2}$.

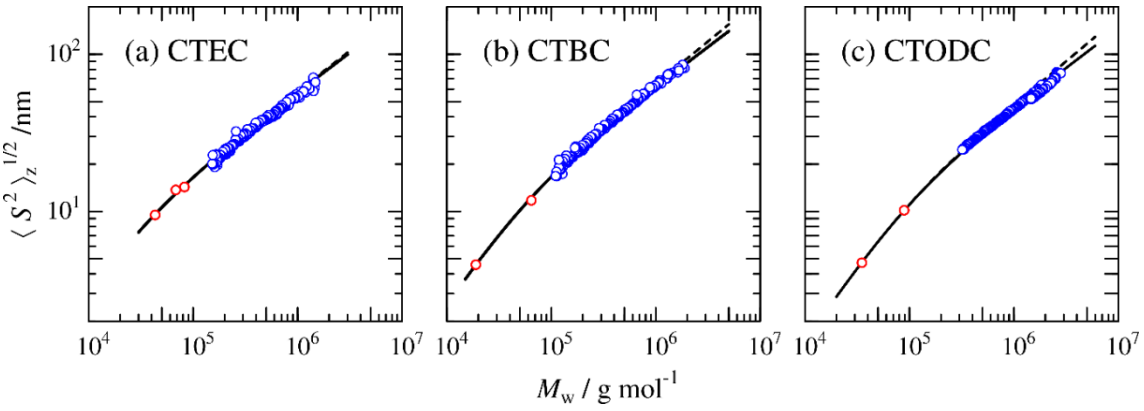

Figure III-4. M_w dependence of $\langle S^2\rangle_z^{1/2}$ for (a) CTEC, (b) CTBC, and (c) CTODC in THF at 25 °C. Blue and red circles are the experimental data determined from SEC-MALS and SAXS measurements, respectively. Solid and dashed curves, theoretical values for the unperturbed and perturbed wormlike chains.

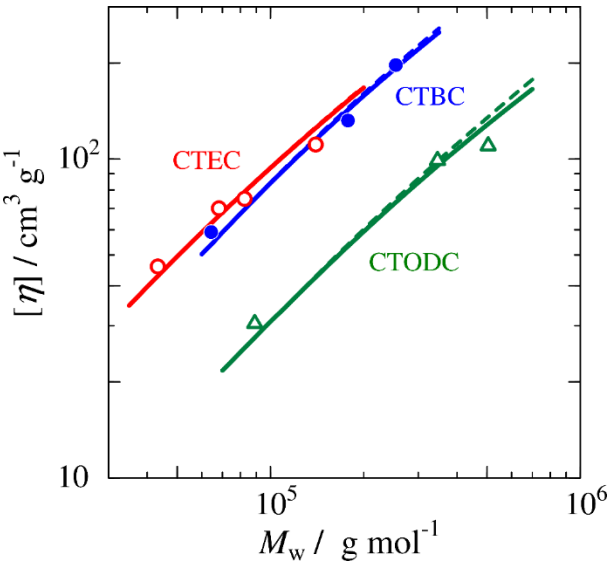

Figure III-5. M_w dependence of $[\eta]$ for CTEC (unfilled circles), CTBC (filled circles), and CTODC (triangles) in THF at 25 °C. Solid and dashed curves, theoretical values for the unperturbed and perturbed wormlike chains.

The Holtzer plots[37] are suitable to analyze the particle scattering function of the semiflexible and rigid polymer chains in solution. The reduced Holtzer plots [M_w q $P(q)$ vs q] for seven cellulose derivative samples in THF are illustrated in Figure III-6. For CTEC and CTBC samples, wide horizontal region so called 'Holtzer plateau' are found at high q range, indicating chain thickness is hardly effectible to the $P(q)$ for the current system while a peak at lower q range reflects the finite chain stiffness. Monotonic increase behavior for CTODC at high q range is most likely due to the low electron density of the side alkyl groups comparing with the main chain and solvent. Similar behavior were also found for some other systems.[38-40]

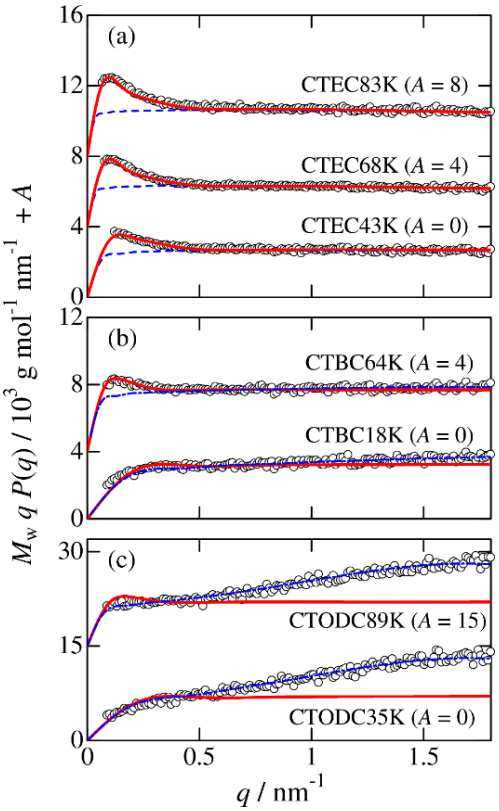

Figure III-6. Reduced Holtzer plots for the indicated CTEC, CTBC, and CTODC samples in THF at 25 °C. The ordinate values are shifted by *A*. Solid red curves, theoretical values for cylindrical wormlike chains with the parameters in Table III-3. Dashed curves in panel (a), theoretical values for rigid cylinders. Dot-dashed curves in panels (b) and (c), theoretical values for core-shell cylinders. See text for the parameters.

III-3-2. Solution IR Spectra

According to Kasat et al.[41, 42] intramolecular hydrogen bonds of C=O groups for 3,5-dimethylphenylcarbamate derivatives of cellulose and amylose are detectable from the amide I band in the IR spectra. We recently determined the number fraction f_{hyd} of hydrogen bonding C=O groups for amylose alkylcarbamates in solution.[26, 27, 33] Figure III-7 shows wavenumber dependence of the molar absorption coefficient ε for CTEC43K, CTBC190K, and CTODC346K in THF at 25 °C. Split amide I bands at 1742 cm^{-1} and 1714 cm^{-1} may be

assigned as free and hydrogen bonding C=O groups. While the wavenumber of the former peak is almost equivalent to the corresponding amylose derivatives, the latter value is quite larger than those for ATEC (1700 cm^{-1}) and ATBC (1698 cm^{-1}), suggesting that the hydrogen bonds of CTEC and CTBC are somewhat weaker than those for the corresponding amylose derivatives. The observed double peaks are well fitted by the two Gaussian distributions as illustrated in the figure and therefore the values of f_{hyd} were estimated to be 0.42 (CTEC), 0.44 (CTBC), and 0.40 (CTODC).

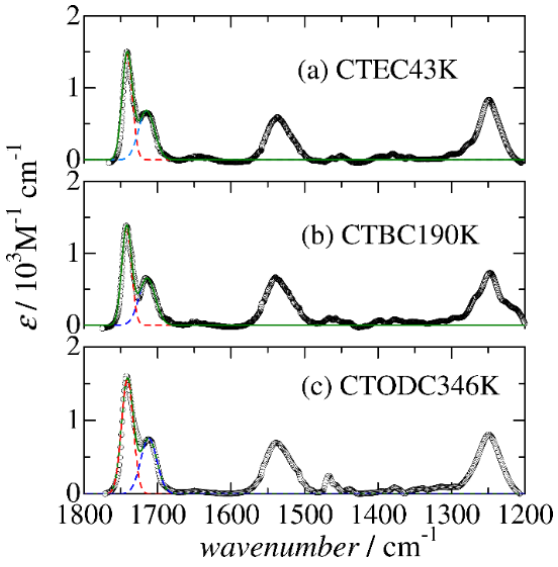

Figure III-7. Solution IR spectra for indicated cellulose carbamate derivative samples in THF at 25 °C.

III-4. Discussion

III-4-1. Analyses in Terms of the Wormlike Chain Model

All the dimensional and hydrodynamic properties summarized in the former section have a typical feature of rigid and/or semiflexible polymer chains. We thus analyzed the data in terms of the conventional Kratky-Porod wormlike chain model,[8] which is a special case of the helical wormlike chain.[43] According to Benoit and Doty,[43, 44] theoretical gyration radius $\langle S^2 \rangle_0$ for the unperturbed wormlike chain is calculated by the following equation

$$\left\langle S^2 \right\rangle_0 = \frac{L}{6\lambda} - \frac{1}{4\lambda^2} + \frac{1}{4\lambda^3 L} - \frac{1}{8\lambda^4 L^2}\left[1 - \exp\left(-2\lambda L\right)\right] \qquad \text{(III-1)}$$

where L is the contour length and λ^{-1} is the Kuhn segment length. The former parameter should be proportional to the molar mass M of the polymer and the relationship can be written as $L = M / M_L$ with M_L being the molar mass per unit contour length. The two wormlike chain parameters, M_L and λ^{-1}, were unequivocally determined from the curve fitting procedure and summarized in Table III-3. The resultant theoretical solid curves in Figure III-4 successfully reproduce the experimental data. The intramolecular excluded volume effects might not be negligible in the present case because the Kuhn segment number n_K ($\equiv \lambda L$) for the highest molar mass are 100, 60, and 60 for CTEC, CTBC, and CTODC. These values are slightly larger than that for the threshold value (n_K = 50) at which the excluded volume effects become not negligible for neutral polymers (other than polyelectrolytes) in solution.[45, 46] This effect can be estimated by the Domb-Barrett equation[47] in the quasi-two-parameter (QTP) theory,[43, 48, 49] which is established both for flexible and semiflexible polymer chains in solution.[43, 45, 50] The theoretical radius of gyration of the wormlike chains $\langle S^2 \rangle$ in good solvent can be written as

$$\left\langle S^2 \right\rangle = \alpha_s^{\,2} \left\langle S^2 \right\rangle_0 \qquad \text{(III-2)}$$

The radius expansion factor α_s can be calculated with the parameters of λ, M_L, and the excluded volume strength B as a function of M. The last parameter B is roughly estimated in terms of the QTP scheme from the A_2 data to be 0.2, 1.4, and 2.4 nm for CTEC, CTBC, and CTODC. The calculated $\langle S^2 \rangle$ shown as the dashed curves in Figure III-4 are only slightly larger than those for the corresponding unperturbed values (solid curves) if we chose the B values from A_2. We thus conclude that the excluded volume effects are insignificant for the current $\langle S^2 \rangle$ data.

Table III-3. The Molar Mass per Unit Contour Length M_L, the Kuhn Segment Length λ^{-1}, and the Chain Diameter d for CTEC, CTBC, and CTODC from the Different Methods.

Polymer	Method	M_L / nm^{-1} g mol^{-1}	λ^{-1} / nm	d / nm
CTEC	$\langle S^2 \rangle_z$	850 ± 20	17 ± 1	
	$P(q)$	830 ± 70	16 ± 1	0.6 ± 0.2
	$[\eta]$	840[a]	16.5[a]	1.3
CTBC	$\langle S^2 \rangle_z$	1150 ± 50	25 ± 1	
	$P(q)$	1230 ± 30	25[a]	
	$[\eta]$	1150[a]	25[a]	2.5
CTODC	$\langle S^2 \rangle_z$	1850 ± 170	24 ± 3	
	$P(q)$	2230 ± 150	24[a]	
	$[\eta]$	2040[a]	24[a]	3

[a] Assumed.

The particle scattering function $P(q)$ determined by SAXS for relatively low M_w samples were analyzed in terms of the Nakamura-Norisuye expression[51] for the cylindrical wormlike

chains. Three parameters, L, λ^{-1}, and the diameter of the cylinder d, were uniquely determined by a curve fitting procedure for the three CTEC samples as shown in Figure III-6. The appreciable difference of the theoretical values between wormlike cylinder (solid curve) and the rigid cylinder (dashed curves) with the same L and d indicates the accuracy of λ^{-1}. Substantially the same theoretical values were obtained (not shown) if we calculate theoretical z-average particle scattering function with $Đ$ assuming log-normal distribution.

In the case of the $P(q)$ data for CTBC and CTODC, peaks at low-q range are less significant than those for CTEC samples. This is because the Kuhn segment number of these samples are estimated to be between 0.6 and 2.2 from the above-mentioned wormlike chain parameters while those for CTEC samples are higher (3.0 – 5.7), suggesting the finite flexibility are hardly effectible the $P(q)$ data. Although monotonically increase behavior of $qP(q)$ at higher q range cannot be explained by the cylindrical wormlike chains, it can be explained by the concentric double cylinder proposed by Livsey.[52] The particle scattering function of the model can be expressed as

$$P(q) = \int_0^{\pi/2} \left[\frac{d_o^2 G(q,\theta,d_o) + f d_i^2 G(q,\theta,d_i)}{d_o^2 + f d_i^2} \right]^2 \sin\theta \, \mathrm{d}\theta \qquad \text{(III-3)}$$

with

$$G(q,\theta,d_x) = \frac{\sin\left[(qL/2)\cos\theta\right] J_1\left[(qd_x/2)\sin\theta\right]}{\left[(qL/2)\cos\theta\right]\left[(qd_x/2)\sin\theta\right]} \qquad \text{(III-4)}$$

and

$$f = \frac{\Delta\rho_i - \Delta\rho_o}{\Delta\rho_o} \qquad \text{(III-5)}$$

where d_i and d_o are the diameter of the inner (or core) and outer (or shell) cylinders, $\Delta\rho_i$ and $\Delta\rho_o$ are the corresponding excess electron densities, and J_1 is a first-order Bessel function. If

we choose appropriate parameters, that is, L, d_i, d_o, and f (see Supporting information for the parameters), at least L may be unequivocally determined. The mean M_L value from the resultant L for different M_w samples are listed in Table III-3. Somewhat smaller M_L values determined from $\langle S^2 \rangle$ is likely due to the coarse-grained model or the molecular weight distribution. The theoretical dot-dashed curves in Figure III-6 successfully reproduce the experimental data other than the low q region of CTBC64K owing to the chain flexibility. Indeed, the theoretical values (solid curves) for a thin wormlike chain ($d = 0$) with the same λ^{-1} from $\langle S^2 \rangle$ fairly explain the experimental $P(q)$ at $q < 0.5$ nm^{-1}. It should be noted that the discrepancy in the range of $q > 0.5$ nm^{-1} is likely due to the above-mentioned heterogeneous electron density profile in the thickness direction, thus reasonable.

Intrinsic viscosity $[\eta]$ data were analyzed in a similar way of $\langle S^2 \rangle$. Theoretical values of wormlike cylinders in the unperturbed state can be calculated in terms of the Yamakawa-Fujii-Yoshizaki theory[43, 53, 54] with the three parameters of M_L, λ^{-1}, and d at fixed M. If we assume the mean M_L and λ^{-1} from $\langle S^2 \rangle_z$ and $P(q)$, the last parameter d may be determined from the curve fitting procedure (solid curve in Figure III-5) and the resultant values are shown in Table III-3. The excluded volume effects on $[\eta]$ is insignificant if we estimate viscosity expansion factor α_η^3 by means of the QTP scheme[43, 48, 49] with the Barrett equation;[55] note that we utilized the excluded volume strength estimated from A_2 as is the case with $\langle S^2 \rangle_z$. The resultant theoretical values plotted as dashed curves in Figure III-5 are mostly the same as those for the corresponding unperturbed values (solid curves). The obtained chain thickness is reasonable because they are fairly close to the corresponding amylose derivatives (d = 1.6 nm for ATEC,[27] and 2.5 nm for ATBC[26] determined by $[\eta]$). We may therefore conclude that the three physical properties, that is, $\langle S^2 \rangle_z$, $P(q)$, and $[\eta]$, are consistently explained by the current theories for the wormlike chains. In other words, we successfully determined the wormlike chain parameters of the three cellulose alkylcarbamates with reasonable accuracy. The mean values of the

wormlike chain parameters are summarized in Table III-4 along with f_{hyd}. The helix pitch (or helix rise) per residue h was calculated from M_L with the relationship of $h = M_0 / M_L$ with M_0 being the molar mass of the repeat unit. This table includes literature values for cellulose tris(phenylcarbamate) (CTPC),[6] amylose carbamate derivatives,[26, 27, 29, 56] and curdlan tris(phenylcarbamate) (CdTPC).[57]

Table III-4. Comparison of λ^{-1}, Helix Pitch per Residue h, and Number Fraction of Intramolecular Hydrogen Bonding C=O Groups f_{hyd} for Polysaccharide Carbamate Derivatives in THF (or 1,4-dioxane) at 25 °C.

Main chain	*Polymer*	λ^{-1} / *nm*	*h* / *nm*	f_{hyd}	*Ref.*
β-1,4-glucan	CTEC	16.5 ± 1	0.45 ± 0.02	0.42	This work
β-1,4-glucan	CTBC	25 ± 1	0.40 ± 0.02	0.44	This work
β-1,4-glucan	CTODC	24 ± 1	0.51 ± 0.03	0.40	This work
β-1,4-glucan	CTPC [a]	21 ± 2	0.50 ± 0.04	–	6
α-1,4-glucan	ATEC	33 ± 3	0.36 ± 0.02	0.46	27
α-1,4-glucan	ATBC	75 ± 5	0.26 ± 0.01	0.52	26
α-1,4-glucan	ATHC	75 ± 2	0.29 ± 0.02	0.53	27
α-1,4-glucan	ATPC [b]	22 ± 2 [e]	0.34 ± 0.02 [e]	–	29
α-1,4-glucan	AAPC [c]	21 ± 2 [e]	0.34 ± 0.02 [e]	–	56
β-1,3-glucan	CdTPC [d]	57 ± 5	0.39 ± 0.02	–	57

[a] Cellulose tris(phenylcarbamate). [b] Amylose tris(phenylcarbamate). [c] Amylose-2-acetyl-3,6-bis(phenylcarbamate). [d] Curdlan tris(phenylcarbamate). [e] In 1,4-dioxane.

III-4-2. Main Chain and Side Group Dependent Local Helical Structure and Chain Stiffness

The obtained chain stiffness of CTBC is 50 % larger than that for CTEC and the h value is smaller than those for the other cellulose derivatives. This is similar behavior of the corresponding amylose derivatives. We may thus presume that the local helical structure of CTBC may be somewhat tighter than those for the other cellulose carbamate derivatives as in the case of ATBC. Slightly higher f_{hyd} of CTBC supports this suggestion. Another significant aspect is that CTODC has relatively large h and λ^{-1} values while f_{hyd} is somewhat smaller than those for CTEC and CTBC. This is most likely because bulkier side groups both extend and stiffen the main chain of CTODC, considering that similar main chain stiffening were found for other polymers, such as polymethacrylates,[58] polyolefins,[59] and polysilanes.[60, 61] If we compare the main chain dependence of the chain stiffness, cellulose derivatives (CTEC, CTBC, and CTPC) have similar or smaller chain stiffness λ^{-1} and fewer intramolecular hydrogen bonds (f_{hyd}) than those for the corresponding amylose (ATEC, ATBC, and ATPC) and curdlan derivatives (CdTPC) (see also 57). This indicates that cellulose main chain (β-1,4-glucan) does not tend to form regular helical structure comparing with amylose (α-1,4-glucan) and curdlan (β-1,3-glucan). The local helical structure of cellulose derivatives has indeed more extended (h = 0.40 – 0.51 nm) than those for amylose (0.26 – 0.36 nm) and curdlan (0.39 nm). The worse solubility of cellulose alkylcarbamates, especially, CTEC and cellulose tris(*n*-hexylcarbamate) (CTHC), is possibly due to the hydrogen bonding feature because the residual free polar groups of cellulose alkylcarbamates may tend to form intermolecular hydrogen bonds with other polymer chains.

III-5. Conclusion

The Kuhn segment length λ^{-1}, the helix pitch per residue h, and number fraction of intramolecular hydrogen bonds of C=O groups f_{hyd} were determined for three cellulose alkylcarbamates (CTEC, CTBC, and CTODC) with different alkyl side chain length. The chain stiffness of CTBC has higher than that for CTEC as is the case with amylose derivatives, suggesting length of alkyl side chains plays an important role to form local helical structure. On the other hand, bulkier side groups of CTODC tend to stiffen and extend the main chain. The range of chain stiffness of investigated cellulose derivatives are in the range between 16 and 25 nm, which do not exceed the values known for cellulose and other cellulose derivatives as mentioned in Introduction. These results indicate that the intramolecular hydrogen bonds between NH and C=O groups on the neighboring repeat units of cellulose alkylcarabamate derivatives somewhat stiffen the main chain but it is still insignificant comparing with other polysaccharide carbamate derivatives, that is, amylose and curdlan.

References

1. W. Burchard, Light Scattering from Polysaccharides as Soft Materials. In: Borsali R and Pecora R, editors. Soft Matter Characterization: Springer Netherlands, **2008**. pp. 463-603.

2. W. Burchard, E. Husemann, *Makromol. Chem.* **1961**, 44, 358-387.

3. W. Burchard, *Makromol. Chem.* **1965**, 88, 11-28.

4. A. K. Gupta, E. Marchal, W. Burchard, H. Benoit, *Polymer* **1976**, 17, 363-366.

5. J. Daňhelka, M. Netopilíak, M. Bohdanecký, *J. Polym. Sci. Part B: Polym. Phys.* **1987**, 25, 1801-1815.

6. F. Kasabo, T. Kanematsu, T. Nakagawa, T. Sato, A. Teramoto, *Macromolecules* **2000**, 33, 2748-2756.

7. H. Yanai, T. Sato, *Polym. J.* **2006**, 38, 226-233.

8. O. Kratky, G. Porod, *Recl. Trav. Chim. Pays-Bas* **1949**, 68, 1106-1122.

9. T. Norisuye, A. Tsuboi, T. Sato, A. Teramoto, *Macromol. Symp.* **1997**, 120, 65-76.

10. A. Tsuboi, M. Yamasaki, T. Norisuye, A. Teramoto, *Polym. J.* **1995**, 27, 1219-1229.

11. A. Tsuboi, T. Norisuye, A. Teramoto, *Macromolecules* **1996**, 29, 3597-3602.

12. T. Ikai, Y. Okamoto, *Chem. Rev* **2009**, 109, 6077-6101.

13. Y. Okamoto, M. Kawashima, K. Hatada, *J. Chromatogr A* **1986**, 363, 173-186.

14. E. Bianchi, A. Ciferri, G. Conio, A. Cosani, M. Terbojevich, *Macromolecules* **1985**, 18, 646-650.

15. C. L. McCormick, P. A. Callais, B. H. Hutchinson, *Macromolecules* **1985**, 18, 2394-2401.

16. K. Kamide, M. Saito, K. Kowsaka, *Polym. J.* **1987**, 19, 1173-1181.

17. W. Burchard, N. Habermann, P. Klüfers, B. Seger, U. Wilhelm, *Angewandte Chemie International Edition in English* **1994**, 33, 884-887.

18. B. Seger, T. Aberle, W. Burchard *Carbohydr Polym.* **1996**, 31, 105-112.

19. K. Saalwachter, W. Burchard, P. Klufers, G. Kettenbach, P. Mayer, D. Klemm, S. Dugarmaa, *Macromolecules* **2000**, 33, 4094-4107.

20. J. P. Zhou, L. N. Zhang, J. Cai *J. Polym. Sci, Part B: Polym Phys* **2004**, 42, 347-453.

21. M. Yanagisawa, A. Isogai *Biomacromolecules* **2005**, 6, 1258-1265.

22. J. Cai, Y. T. Liu, L. N. Zhang, *J. Polym. Sci, Part B: Polym Phys* **2006**, 44, 3093-3101.

23. M. Kes, B. E. Christensen, *J. Chromatogr A* **2013**, 1281, 32-37.

24. S. V. Bushin, A. K. Khripunov, M. A. Bezrukova, E. P. Astapenko, *Polymer Science Series A* **2007**, 49, 71-76.

25. J. W. Mays, *Macromolecules* **1988**, 21, 3179-3183.

26. K. Terao, M. Murashima, Y. Sano, S. Arakawa, S. Kitamura, T. Norisuye, *Macromolecules* **2010**, 43, 1061-1068.

27. K. Terao, F. Maeda, K. Oyamada, T. Ochiai, S. Kitamura, T. Sato, *J. Phys. Chem. B* **2012**, 116, 12714-12720.

28. Y. Nakanishi, T. Norisuye, A. Teramoto, S. Kitamura, *Macromolecules* **1993**, 26, 4220-4225

29. K. Terao, T. Fujii, M. Tsuda, S. Kitamura, T. Norisuye *Polym. J.* **2009**, 41, 201-207.

30. C. L. McCormick, P. A. Callais, *Polymer* **1987**, 28, 2317-2323.

31. V. Schurig, J. Zhu, V. Muschalek *Chromatographia* **1993**, 35, 237-240.

32. T. Kubota, C. Yamamoto, Y. Okamoto, *J. Am. Chem. Soc.* **2000**, 122, 4056-4059.

33. Y. Sano, K. Terao, S. Arakawa, M. Ohtoh, S. Kitamura, T. Norisuye *Polymer* **2010**, 51, 4243-4248.

34. G. C. Berry, *J. Chem Phys* **1966**, 44, 4550-4564.

35. K. Terao, J. W. Mays Eur, *Polym J.* **2004**, 40, 1623-1627.

36. X. Y. Jiang, K. Terao, W. J. Chung, M. Naito, *Polymer* **2015**, 68, 221-226.

37. A. Holtzer, *J. Polym. Sci.* **1955**, 17, 432-434.

38. P. Hickl, M. Ballauff, U. Scherf, K. Mullen, P. Linder, *Macromolecules* **1997**, 30, 273-279.

39. K. Terao, K. Mizuno, M. Murashima, Y. Kita, C. Hongo, K. Okuyama, T. Norisuye, H. P. Bächinger, *Macromolecules* **2008**, 41, 7203-7210.

40. S. Arakawa, K. Terao, S. Kitamura, T. Sato, *Polym. Chem.* **2012**, 3, 472-478.

41. R. B. Kasat, Y. Zvinevich, H. W. Hillhouse, K. T. Thomson, N. H. L. Wang, E. I. Franses, *J. Phys. Chem. B* **2006**, 110, 14114-14122.

42. R. B. Kasat, S. Y. Wee, J. X. Loh, N. H. Wang, E. I. Franses, *Journal of chromatography B, Analytical technologies in the biomedical and life sciences* **2008**, 875, 81-92.

43. H. Yamakawa, T. Yoshizaki, *Helical Wormlike Chains in Polymer Solutions, 2nd ed.* Springer: Berlin, Germany, 2016.

44. H. Benoit, P. Doty, *J. Phys. Chem.* **1953**, 57, 958-963.

45. T. Norisuye, A. Tsuboi, A. Teramoto *Polym. J.* **1996**, 28, 357-361.

46. T. Norisuye, H. Fujita *Polym. J.* **1982**, 14, 143-147.

47. C. Domb, A. J. Barrett, *Polymer* **1976**, 17, 179-184.

48. H. Yamakawa, W. H. Stockmayer, *J. Chem. Phys.* **1972**, 57, 2843-2854.

49. J. Shimada, H. Yamakawa, *J. Chem. Phys.* **1986**, 85, 591-600.

50. Y. Nakamura, T. Norisuye 2.02 - Polymer Properties in Solutions. In: Editors-in-Chief: Krzysztof M and Martin M, editors. Polymer Science: A Comprehensive Reference. Amsterdam: Elsevier, **2012**. pp. 5-32.

51. Y. Nakamura, T. Norisuye, *J. Polym. Sci, Part B: Polym. Phys.* **2004**, 42, 1398-1407.

52. I. Livsey, *Journal of the Chemical Society-Faraday Transactions Ii* **1987**, 83, 1445-1452.

53. H. Yamakawa, M. Fujii, *Macromolecules* **1974**, 7, 128-135.

54. H. Yamakawa, T. Yoshizaki, *Macromolecules* **1980**, 13, 633-643.

55. A. J. Barrett, *Macromolecules* **1984**, 17, 1566-1572.

56. M. Tsuda, K. Terao, S. Kitamura, T. Sato, *Biopolymers* **2012**, 97, 1010-1017.

57. T. Ochiai, K. Terao, Y. Nakamura, C. Yoshikawa, T. Sato, *Polymer* **2012**, 53, 3946-3950.

58. Z. Xu, N. Hadjichristidis, L. J. Fetters, *Macromolecules* **1984**, 17, 2303-2306.

59. L. J. Fetters, D. J. Lohse, C. A. Garcia-Franco, P. Brant, D. Richter, *Macromolecules* **2002**, 35, 10096-10101.

60. M. Fujiki, J. R. Koe, Terao K., Sato T., A. Teramoto, J. Watanabe, *Polym. J.* **2003**, 35, 297-344.

61. W. J. Chung, H. Shibaguchi, K. Terao, M. Fujiki, M. Naito, *Macromolecules* **2011**, 44, 6568-6573.

Appendix. Attenuated Total Reflection Infrared Spectroscopy

The ATR-IR spectra were recorded in the range between 400 and 4000 cm^{-1} on an FT/IR-6100 with ATR PRO 410-S (JASCO) using a diamond-ZnSe ATR crystal. About 2-3 mg of all the samples was placed on the surface of the ATR crystal (diameter, 2mm). All spectra were obtained from 128 scans with a resolution of 4 cm^{-1}.

Figure IIIA-1 shows wavenumber dependence of reflectance for CTEC, CTBC, and CTODC. Absorption peak around 3000-2800 cm^{-1} attributing to C-H stretching vibration, and peak around 3500-3200 cm^{-1} attributing to N-H stretching vibration. The spectra for each sample with four different M_w are overlapped closely, indicate that they have the same chemical structure.

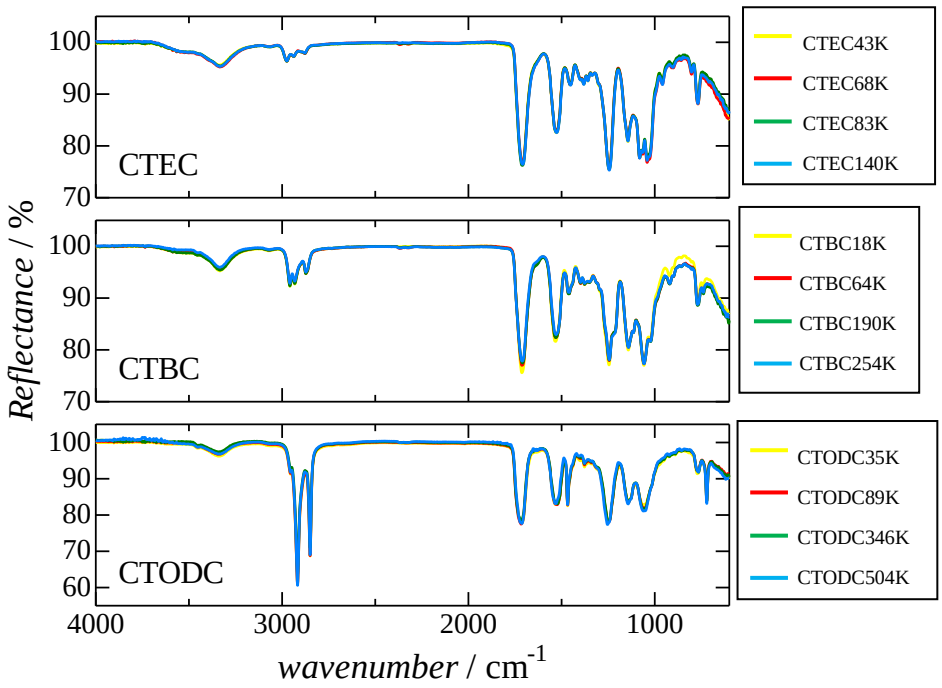

Figure IIIA-1. ATR-IR spectra for indicated cellulose carbamate derivative samples

Chapter IV.

Chain Stiffness of Cellulose Tris(phenylcarabamate) in Tricresyl Phosphate (TCP)

IV-1. Introduction

Since cellulose tris(phenylcarbamate) (CTPC) is easily synthesized from natural cellulose[1,2] and soluble in many common organic solvents including theta solvents,[3] much work has been done for dilute solution properties to elucidate the conformational characteristics of cellulosic chains.[1,4-13] Almost all reports indicate that CTPC behaves as a semiflexible polymer in solution. Although conformational properties and intermolecular interactions of semiflexible polymers are widely investigated,[14-17] comprehensive study through rheological and conformational properties are not still enough to elucidate the relationship including cellulose.[18] This is likely because suitable solvent is different between these properties, namely, low viscous and volatile organic solvents were favorably used to determine their conformation in solution whereas high viscous solvents with low vapor pressure are suitable to characterize polymer dynamics. As a preliminary study of this research, we found that CTPC is well soluble in tricresyl phosphate (TCP), which is a useful solvent to investigate rheological properties and indeed dynamic birefringence and viscoelasticity of polystyrene in this solvent are investigated in detail[19]. As a step of the comprehensive work of static and dynamic properties of semiflexible polymers in solution, we report dimensional properties for CTPC in TCP in this chapter.

Regarding to the chain stiffness of CTPC in solution, Dañhelka et al.[10] analyzed their own and elder data[4,7,9,8] to determine the chain stiffness parameter λ^{-1} (Kuhn segment length or twice of persistence length) of the Kratky-Porod wormlike chain[20] in different solvent conditions. While λ^{-1} for CTPC in tetrahydrofuran (THF), acetone, dioxane, and pyridine at the temperatures T of 20 or 25 °C was reported to be in a rather narrow range from 19 to 27 nm,

the parameter in benzophenone, cycohexanol, and anisol was much smaller, that is, 7 – 10 nm at relatively high temperatures (73 – 94 °C). Even though we consider the known temperature dependence of CTPC in four different solvents, that is, $d \ln\lambda^{-1} / dT \sim -6.5 \times 10^{-3}$ K^{-1},[13,21] the chain stiffness in the latter three solvents was found to be smaller than those in the former solvents. The solvent dependent conformation suggests that the intramolecular hydrogen bonding interactions and/or polymer-solvent interactions play an important role to determine the conformation of CTPC in dilute solution as pointed out by Sutter et al.[9]. We also showed that local helical structure stabilized by the intramolecular hydrogen bonds between the carbamate groups on the neighboring repeat units stiffen the main chain of cellulose tris(alkylcarbamate)s (Chapter III), curdlan tris(phenylcarbamate) [22] and amylose tris(alkylcarbamate)s[23-25] and furthermore hydrogen bonding solvent molecules significantly extend and stiffen the main chain of amylose tris(phenylcarbamate) and amylose tris(3,5-dimethylphenylcarbamate)[26,27]. The chain conformation of CTPC in arbitrary solvent cannot therefore be predicted without determining it directly in solution.

We thus made small-angle X-ray scattering (SAXS) measurements for two CTPC samples in TCP to determine the chain stiffness parameter because conventional light scattering measurements are not suitable for this purpose because of the difficulty of optical clean and very small contrast factor of visible light. Indeed, dimensional properties of polystyrene in TCP were investigated by means of neutron scattering[28] and those for polysaccharides in an ionic liquid were studied by SAXS (Chapter II) due to the same reason.

IV-2. Experimental

IV-2-1. Samples and Test Solutions

Laboratory stored two CTPC samples originally synthesized and fractionated for the former study[11] were chosen and designated to be CTPC61K and CTPC84K. Their weight-average

molar mass M_w and the dispersity index $Đ$ defined as the ratio of M_w to the number-average molar mass were determined to be $M_w = 6.08 \times 10^4$ g mol^{-1} and $Đ = 1.1$ for CTPC61K and $M_w = 8.41 \times 10^4$ g mol^{-1} and $Đ = 1.1$ for CTPC84K from SEC-MALS measurements in THF. The details of the measurement were as reported in Chapter III and the literature value[11] of the refractive index increment was used to analyze the light scattering intensity. The validity of the M_w values was confirmed by the intrinsic viscosity $[\eta]$ in THF at 25 °C with the known $[\eta] - M_w$ relationship.[11] The weight-average number of repeat unit N_w was thus evaluated to be 117 and 162 for CTPC61K and CTPC84K, respectively.

TCP was purchased from Kishida and used as a solvent without further purification. Each sample which was dried in vacuum at room temperature overnight was weighed with an electronic balance in a glass bottle and an appropriate amount of solvent was added before at least 48 hours prior to use for the following measurements.

IV-2-2. Small angle X-ray scattering (SAXS) measurements

SAXS measurements were carried out at the BL40B2 beamline in SPring-8 (Hyogo, Japan) with the approval of the Japan Synchrotron Radiation Research Institute (JASRI) (Proposal Nos. 2014B1087, 2015A1179, 2015B1100, and 2015B1674) to determine scattering intensities $I(q)$ at 25 °C for pure TCP and four CTPC solutions having different polymer mass concentration c between 1×10^{-2} g cm^{-3} and 5×10^{-2} g cm^{-3}. Although the highest concentration is about twice higher than the overlap concentration, good linearity of the Berry plot in the wide concentration range was reported for CTPC in THF[11]. Test solutions or solvent were measured in the same quartz capillary cell with a diameter of 2 mmϕ. The obtained two-dimensional image data were analyzed in terms of the circular average method to determine $I(q)$ as a function of the magnitude q of the scattering vector. The wavelength, camera length, and accumulation time were chosen to be 0.10 nm, 4000 mm, and 300 s, respectively. The

obtained $I(q)$ was normalized by the intensity of the direct beam at the lower end of the capillary to calibrate both intensity of the incident light and the transmittance of X-ray through the cell including solution to determine the excess scattering intensity $\Delta I(q)$ from the solute.

IV-3. Results and Discussion

The Berry square-root plots[29] for the two CTPC samples in TCP at 25 °C are displayed in Figure IV-1 to extrapolate the scattering intensity to infinite dilution and to $q^2 = 0$. The z-average mean-square radius of gyration $\langle S^2 \rangle_z$ and the second virial coefficient A_2 are determined from the corresponding initial slopes; note that the optical constant was estimated from the doubly extrapolated value $[c/\Delta I(0)]_{c=0}^{1/2}$ with the method reported in ref[30]. The resultant $\langle S^2 \rangle_z$ and A_2 data are listed in Table IV-1 along with the M_w values from the SEC-MALS measurements. The quite large positive A_2 indicates that TCP is a good solvent of CTPC.

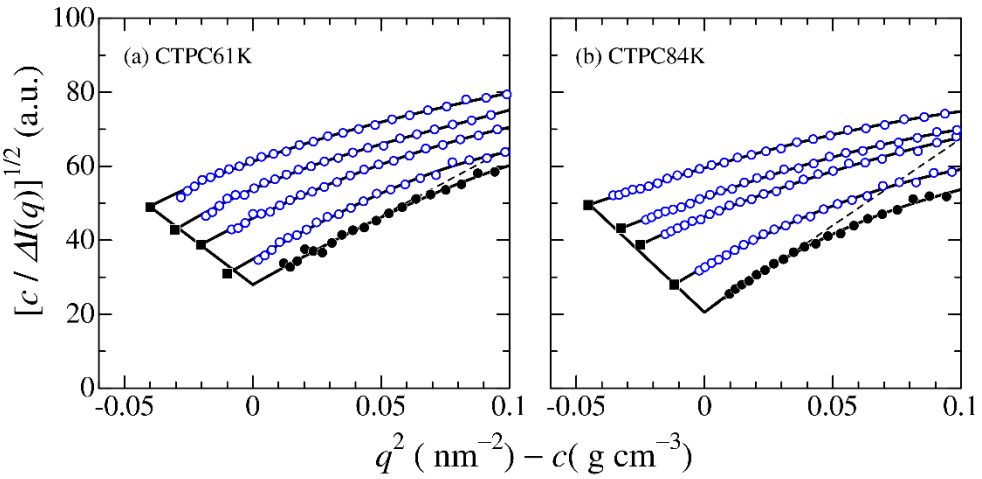

Figure IV-1. Square root Zimm plots (Berry plots) for CTPC61K (a) and CTPC84K (b) in TCP at 25 °C. Filled circles and squares, extrapolated values to $c = 0$ and $q^2 = 0$, respectively.

Table IV-1. Molecular Characteristics of CTPC Samples in TCP at 25 °C.

Samples	M_w (10^4 g mol^{-1})	$\langle S^2\rangle_z^{1/2}$ (nm)	$\langle S^2\rangle_{calc}^{1/2}$	A_2 (10^{-4} mol cm^3 g^{-2})
CTPC61K	6.08	8.8	9.0	1.4
CTPC84K	8.41	11.5	11.7	1.5

[a] Calculated by eq IV-3 with the parameters in Table IV-2

The particle scattering function $P(q)$ defined as $[\Delta I(q) / \Delta I(0)]_{c=0}$ for each sample was also obtained from the $\Delta I(q)$ data with the extrapolated value $[c/\Delta I(0)]_{c=0}$. Figure IV-2 illustrates the reduced Holtzer plots in which the flat plateau is found for each sample at higher q range with an appreciable peak at low q. This is a typical feature of the wormlike chain. Slight decrease of $qP(q)$ at the highest q region in the figure may be due to the chain thickness effect. We thus analyzed the $P(q)$ data in terms of the touched-bead wormlike chain with the bead diameter d is expressed as[31,32]

$$P(q) = 9\left(\frac{2}{qd}\right)^6 \left(\sin\frac{qd}{2} - \frac{qd}{2}\cos\frac{qd}{2}\right)^2 P_0(q) \qquad \text{(IV-1)}$$

Here, $P_0(q)$ is the particle scattering function of the thin wormlike chain, which is characterized by λ^{-1} and the contour length L. It is related to the characteristic function $I(\lambda^{-1}q; \lambda t)$ of the wormlike chain as follows

$$P_0(q) = \frac{2}{L^2}\int_0^L (L-t)\, I\left(\lambda^{-1}q; \lambda t\right) dt \qquad \text{(IV-2)}$$

In this study we used the approximate expression by Nakamura and Norisuye[33,34] to calculate $I(\lambda^{-1}q; \lambda t)$. The three parameters were unequivocally determined by means of the curve fitting procedure. Theoretical curves in Figure IV-2 calculated with the obtained parameters in Table IV-2 successfully reproduce the experimental data. The radii of gyration $\langle S^2\rangle_{calc}$ calculated from the following Benoit-Doty equation[35]

$$\langle S^2 \rangle_{\text{calc}} = \frac{L}{6\lambda} - \frac{1}{4\lambda^2} + \frac{1}{4\lambda^3 L} - \frac{1}{8\lambda^4 L^2}\left[1 - \exp(-2\lambda L)\right] \qquad \text{(IV-3)}$$

with the parameters in Table IV-2 are listed in the fourth column in Table IV-1; note that both the chain thickness effect and the excluded volume effect should be negligible on $\langle S^2 \rangle_{\text{calc}}$ because of $L > 50\,d$ [36] and $\lambda L < 8$[37]. The resultant $\langle S^2 \rangle_{\text{calc}}$ values are almost equivalent to the corresponding experimental $\langle S^2 \rangle_{\text{z}}$. Furthermore, the helix pitch per residue h defined as L/N_{w} was calculated to be 0.51 ± 0.03 nm, which is substantially the same as those for CTPC in other solvents[10,11,38] and for the crystal structure of CTPC-2-butanone complex[39]. We may thus conclude that both $\langle S^2 \rangle_{\text{z}}$ and $P(q)$ data for CTPC in TCP are consistently explained by the wormlike chain model.

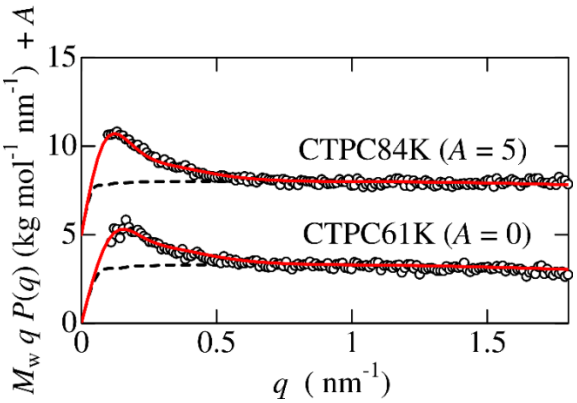

Figure IV-2. Reduced Holtzer plots for CTPC in TCP at 25 °C. Solid and dashed curves indicate the theoretical values for the touched bead wormlike chain and the touched bead rigid rod, respectively.

Table IV-2. Wormlike Chain Parameters for CTPC Samples in TCP at 25 °C.

sample	L (nm)	λ^{-1} (nm)	d (nm)
CTPC61K	56 ± 3	11.5± 0.5	0.9 ± 0.1
CTPC84K	86 ± 5	11.5± 0.5	0.8 ± 0.1

The obtained wormlike chain parameters are summarized in Table IV-3 with previously reported values in the other solvents. If we assume the above mentioned temperature coefficient [d lnλ^{-1} / dT ~ -6.5×10^{-3} K^{-1}][13,21], the λ^{-1} values in anisol, cyclohexanol, and benzophenone at 25 °C are estimated to be 10 nm, 10 nm, and 14 nm which are quite close to 11.5 nm. It should be noticed that this estimation might have uncertainty since the temperature coefficient for amylose tris(phenylcarbamate)[40] and polystyrene[41] appreciably depend on the solvent. In either case, the present λ^{-1} in TCP (11.5 nm) is quite smaller than the other solvents at 25 °C or 20 °C. We may thus conclude that CTPC has rather high flexibility in the solvents investigated.

Table IV-3. Kuhn Segment Length λ^{-1} for CTPC in Various Solvents.

solvent	T (°C)	λ^{-1} (nm)	h (nm)	Ref.
anisole	94	6.2	0.52 [a]	6,10
cyclohexanol	73	7.6	0.52 [a]	6,10
benzophenone	80	9.6	0.52 [a]	8,10
tricresyl phosphate (TCP)	25	11.5 ± 0.5	0.51	this work
1-methyl-2-pyrrolidone (NMP)	25	16	0.49	38
1% LiCl /1,3-dimethyl-2-imidazolidinone	25	18	0.515 [a]	12
pyridine	20	20	0.52 [a]	4,10
tetrahydrofuran (THF)	25	19 – 24	0.50 – 0.57	10-12
1,4-dioxane / methanol 49/51 (v/v)	25	26	0.515[a]	1,5

[a] Assumed.

IV-4. Conclusion

The chain stiffness and helix pitch per residue are successfully determined from solution SAXS measurements for CTPC in TCP at 25 °C. The obtained chain stiffness parameter is

substantially smaller than those determined around room temperature and similar to those in some polar solvents when we assume the known temperature coefficient. Significant solvent dependence of the conformational properties indicates that the polymer-solvent interaction is important for CTPC chain as is also reported for other polysaccharide phenylcarbamate derivatives.

References

1. W. Burchard, Light Scattering from Polysaccharides as Soft Materials. In: Borsali R and Pecora R, editors. Soft Matter Characterization: Springer Netherlands, **2008**. pp. 463-603.

2. W. M. Hearon, G. D. Hiatt, C.R. Fordyce, *J. Am. Chem. Soc.* **1943**, 65, 829-833.

3. W. Burchard, *Polymer* **1969**, 10, 467-475.

4. W. Burchard, E. Husemann. *Makromol Chem.* **1961**, 44, 358-387

5. W. Burchard, Makromol Chem **1965**, 88, 11-28

6. V. P. Shanbhag, J. Ohman, Arkiv for Kemi **1968**, 29, 163-&

7. J. Ohman, Arkiv for Kemi **1969**, 31, 125-136

8. H. Janeschitz-Kriegl, W. Burchard, *J. Polym. Sci.* A2 **1968**, 6, 1953-1974.

9. W. Sutter, W. Burchard, *Makromol Chem Macromol Chem Phys*, **1978**, 179, 1961-1980

10. J. Daňhelka, M. Netopilíak, M. Bohdanecký, *J. Polym. Sci., Part B: Polym. Phys.*,**1987**, 25, 1801-1815.

11. F. Kasabo, T. Kanematsu, T. Nakagawa, T. Sato, A. Teramoto, *Macromolecules*, **2000**, 33, 2748-2756.

12. M. Yanagisawa, A. Isogai, *Biomacromolecules* **2005**, 6, 1258-1265.

13. H. Yanai, T. Sato, *Polym. J.* **2006**, 38, 226-233.

14. H. Yamakawa, T. Yoshizaki, *Helical Wormlike Chains in Polymer Solutions, 2nd ed.* Springer: Berlin, Germany, 2016.

15. Y. Nakamura, T. Norisuye, 2.02 - Polymer Properties in Solutions. In: Editors-in-Chief: Krzysztof M and Martin M, editors. Polymer Science: A Comprehensive Reference. Amsterdam: Elsevier, **2012**. pp. 5-32.

16. T. Norisuye, *Prog. Polym. Sci.* **1993**, 18, 543-584.

17. R. Koyama, T. Sato, *Macromolecules* **2002**, 35, 2235-2242.

18. A. Maeda, T. Inoue, T. Sato, *Macromolecules* **2013**, 46, 7118-7124.

19. T. Inoue, T. Uematsu, K. Osaki, *Macromolecules* **2002**, 35, 820-826.

20. O. Kratky, G. Porod, *Recl. Trav. Chim. Pays-Bas* **1949**, 68, 1106-1122

21. G. V. Reddy, M. Bohdanecky, *Macromolecules* **1987**, 20, 1393-1396.

22. T. Ochiai, K. Terao, Y. Nakamura, C. Yoshikawa, T. Sato, *Polymer* **2012**, 53, 3946-3950.

23. K. Terao, M. Murashima, Y.Sano, S. Arakawa, S. Kitamura, T. Norisuye, *Macromolecules* **2010**, 43, 1061-1068.

24. Y. Sano, K. Terao, S. Arakawa, M. Ohtoh, S. Kitamura, T. Norisuye, *Polymer* **2010**, 51, 4243-4248.

25. K. Terao, F. Maeda, K. Oyamada, T. Ochiai, S. Kitamura, T. Sato, *J. Phys. Chem. B* **2012**, 116, 12714-12720.

26. T. Fujii, K. Terao, M. Tsuda, S. Kitamura, T. Norisuye, *Biopolymers* **2009**, 91, 729-736.

27. M. Tsuda, K. Terao, Y. Nakamura, Y. Kita, S. Kitamura, T. Sato, *Macromolecules* **2010**, 43, 5779-5784.

28. T. P. Lodge, K. C. Hermann, M. R. Landryt, *Macromolecules* **1986**, 19, 1996-2002

29. G. C. Berry, *J. Chem. Phys.* **1966**, 44, 4550-4564.

30. X. Y. Jiang, K. Terao, W. J. Chung, M. Naito, *Polymer* **2015**, 68, 221-226.

31. K. Nagasaka, T. Yoshizaki, J. Shimada, H. Yamakawa, *Macromolecules* **1991**, 24, 924-931.

32. W. Burchard, K. Kajiwara, *Proc. R. Soc. London, Ser A* **1970**, 316, 185-199.

33. Y. Nakamura, T. Norisuye, *J. Polym. Sci. Part B: Polym. Phys.* **2004**, 42, 1398-1407.

34. Y. Nakamura, T. Norisuye, Brush-Like Polymers. In *Soft Matter Characterization,* Borsali, R.; Pecora, R., Eds. Springer Netherlands: **2008**; pp 235-286

35. H. Benoit, P. Doty, *J. Phys. Chem.* **1953**, 57, 958-963.

36. T. Konishi, T. Yoshizaki, T. Saito, Y. Einaga, H. Yamakawa, *Macromolecules* **1990**, 23, 290-297.

37. T. Norisuye, A. Tsuboi, A. Teramoto, *Polym. J.* **1996**, 28, 357-361.

38. T. Norisuye, A. Tsuboi, T. Sato, A. Teramoto, *Macromol. Symp.* **1997**, 120, 65-76. 39.

39. P. Zugenmaier, U. Vogt, *Makromol. Chem.* **1983**, 184, 1749-1760.

40. N. Asano, S. Kitamura, K. Terao, *J. Phys. Chem. B* **2013**, 117, 9576-9583.

41. K. Terao, N. Morihana, H. Ichikawa, *Polym. J.* **2014**, 46, 155-159.

Chapter V.

Viscoelasticity and Rheo-Optical Study on Cellulose Tris(phenylcarbamate) in Tricresyl Phosphate

V-1. Introduction

To clarify the relationship between the conformation and dynamics of polymers in solution is an important clue to understand the correlation between physical properties and chemical structures of polymers. One has to determine both properties in the same solvent conditions to solve this problem. It is however not easy to study the relationship between the conformation and fast dynamics of polymers, because scattering methods to determine the chain conformation in solution require low viscosity solvents, whereas highly viscous solvents are preferably used to study the fast polymer dynamics.

Recently, Maeda et al. have studied light scattering, viscoelasticity, and rheo-optical measurements of cellulose in ionic liquids to determine the molar mass of the Kuhn segment M_K and that of the Rouse segment M_s. They found that the M_s value is close to M_K for cellulose, being different from previously reported polystyrene in relatively dilute solution.[1-2] This may depend on the difference in the chain stiffness. To elucidate the relationship as a general rule, both M_K and M_s of other polymers in the same solvent should be determined.

Dynamics of polymer chains has been studied mostly on flexible polymers so far while little has been known for the dynamic chain rigidity of rigid polymers. In this Chapter, cellulose tris(phenylcarbamate) (CTPC), which behaves as a typical semiflexible polymer in solution, was use for simultaneous measurements of the dynamic viscoelasticity and birefringence. From the viscoelasticity and birefringence measurements, the Rouse segment size M_s can be obtained. In Chapter IV, the chain stiffness λ^{-1} of CTPC in Tricresyl phosphate (TCP) was determined from small-angle X-ray scattering measurements, and the Kuhn segment size M_K was estimated to be 12,000 g/mol from the product of the volume of λ^{-1} and the molar mass per unit contour length M_L. The estimated M_K and M_s were used to discuss the relationship between the conformation and dynamics.

V-2. Experimental Section.

V-2-1. Materials

Two laboratory stored CTPC samples[3-4] were used for the viscoelasticity and rheo-optical measurements. Weight-average molecular weights M_w and the weight to number-average molecular weight ratios M_w/M_n, determined by SEC-MALS are listed in Table V-1. Tricresyl phosphate (TCP) purchased from Kishida was used as the solvent without further purification. The CTPC sample was dried in a vacuum oven at room temperature overnight. The dried CTPC was dissolved TCP in a vacuum oven at 90 ˚C for 48h to prepared the test solutions.

Table V-1. **Molecular Characteristics of CTPC Samples Used.**

sample	$M_w/10^4$	M_w/M_n
CTPC2040K	204	1.1
CTPC25K	2.5	1.1

V-2-2. Measurements

V-2-2-1. Viscoelasticity

The viscoelastic measurements were carried out by an ARES G2 rheometer (TA Instruments) at various temperatures from -60 °C to 50 °C to obtain the complex shear modulus, $G^* = G' + iG''$, ranging from the terminal flow to the glassy zone with parallel plates fixtures. Here, G' and G'' are the storage and loss moduli, respectively. The diameters of the parallel plates used were 4mm, 8mm, and 25mm. Data obtained at different temperatures were reduced to a reference temperature, –25 ˚C, by the method of reduced variables (frequency-temperature superposition).

V-2-2-2. Birefringence

Simultaneous measurements of stress and flow birefringence under oscillatory shear flow were performed on the solutions with a custom-built rheo-optical apparatus equipped with a He-Ne laser (λ_0 = 633 nm) as the light source to obtain G^* and the complex strain-optical coefficient, $K^* = K' + iK''$. Here, K^* is defined as the complex ratio of the shear birefringence

component of refractive index tensor to strain, and K' and K'' are the real and imaginary parts of the complex strain-optical coefficients, respectively. From the stress-optical rule, SOR, K' and K'' are related to G' and G'' by $K' = CG'$ and $K'' = CG''$, where C is the stress-optical coefficient, being related with anisotropy of polarizability of segment.

V-3. Results and Discussion

V-3-1. Viscoelasticity and Birefringence of CTPC in TCP

Figures V-1 shows the frequency dependence of the complex modulus G^* and the complex strain-optical coefficient K^* for a TCP solution of CTPC25K sample with a concentration of c = 0.0152 g cm^{-3}. In the abscissa, a_T is the temperature-dependent shift factor. The glassy contributions of the solvent was observed for both of G^* and K^* data at high frequencies of $\log(\omega a_T/s^{-1}) > 6$. At low frequencies of $\log(\omega a_T/s^{-1}) < 5$, the weak polymeric contribution is observed in G'. K' and K'' are negative at low frequencies. The sign of K'' changes around $\log(\omega a_T/s^{-1}) = 3$ but the sign of K' keeps negative.

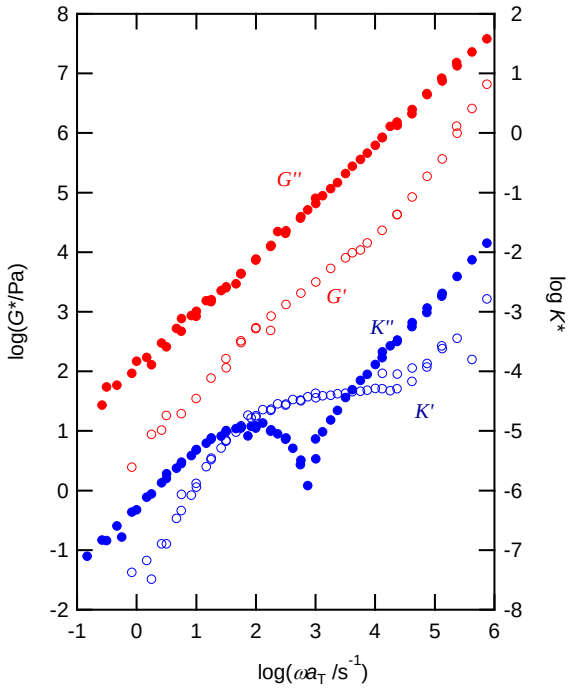

Figure V-1. Frequency dependences of G^* and K^* for a TCP solution of CTPC25K (M_w = 2.5 × 10^4 g mol^{-1}) sample. Reference temperature, T_r, is –25 °C. Concentration, c, is 0.0152g cm^{-3}. Filled black circles: G'; unfilled black circles: G''; filled blue squares: K'; unfilled blue squares: K''.

Figures V-2 shows the frequency dependence of G^* and K^* for a TCP solution of CTPC2040K sample with a concentration of c = 0.0228 g cm^{-3}. At low frequencies, the rubbery plateau region is clearly observed for G^*. Both K' and K'' change the sign from negative to positive around $\log(\omega a_T/s^{-1}) = 3$ and $\log(\omega a_T/s^{-1}) = 5$, respectively. The estimated rubbery plateau modulus, G_N, was 200 Pa.

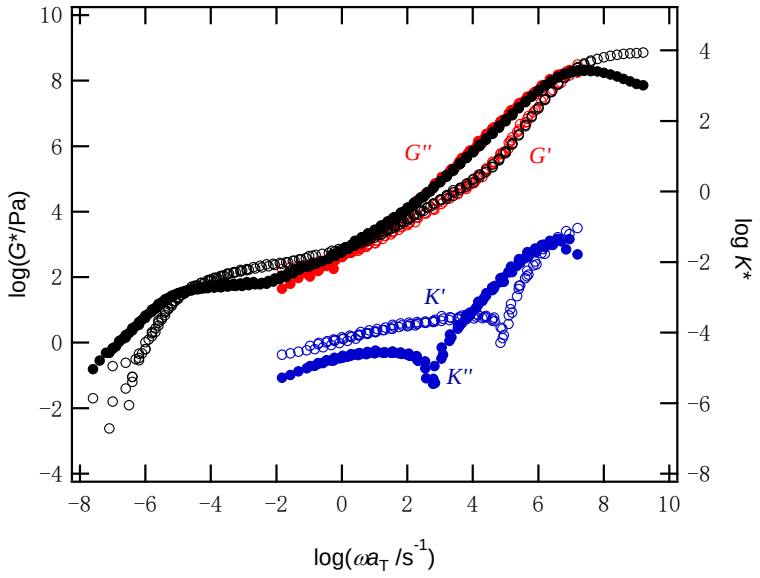

Figure V-2. Frequency dependences of G^* and K^* for a TCP solution of CTPC2K (M_w = 2.04 × 10^6 g mol^{-1}) sample. Reference temperature, T_r, is –25 °C. Concentration, c, is 0.0228g cm^{-3}. Filled and unfilled black circles: G' and G'' obtained by ARES G2, respectively; filled and unfilled red circles: $G'$and G'' obtained by the rheo-optical apparatus, respectively; filled and unfilled blue squares: K' and K'' obtained by the rheo-optical apparatus, respectively.

V-3-2. Various Contributions to the Viscoelastic and Birefringence Responses

According to the theory by Shankar et al.[5-7] for semi flexible chains, the viscoelastic response of the polymer solution is taken as the sum of contributions of orientation G_{ornt}^*, curvature G_{curv}^*, and tensile G_{tens}^* modes of the polymer chain as well as of the solvent G_e^*

$$G^* = G_{ornt}^* + G_{curv}^* + G_{tens}^* + G_e^* \quad \text{(V-1)}$$

On the other hand, the curvature and tensile modes may little contribute to the birefringence response of the polymer solution. Thus, one can write K^* as

$$K^* = K_{\mathrm{ornt}}{}^* + K_{\mathrm{e}}{}^* \qquad \text{(V-2)}$$

where $K_{\mathrm{ornt}}{}^*$ and $K_{\mathrm{e}}{}^*$ are the contributions of the polymer orientation mode and of the solvent to K^*, respectively. Because of a very short relaxation time for the solvent, G'_{e} and K'_{e} are proportional to ω^2, and G''_{e} and K''_{e} are proportional to ω. In Figures V-1 and V-2, G^* and K^* at $4.5 < \log(\omega a_T/\mathrm{s}^{-1}) < 6$, almost obey these frequency dependences, so that $G_{\mathrm{e}}{}^*$ and $K_{\mathrm{e}}{}^*$ are predominant in G^* and K^* in such a frequency region.

For the simplest model, the contribution $G_{\mathrm{ornt}}{}^*$ of the polymer orientation mode is expressed by the Rouse-Zimm theory of the bead-spring model.[8-9] The result is given by

$$G^*_{\mathrm{ornt}}(\omega) = G^*_{\mathrm{RZ}}(\omega) = \frac{cRT}{M}\sum_{p=1}^{n_s}\frac{\mathrm{i}\omega\tau_p}{1+\mathrm{i}\omega\tau_p} \qquad \text{(V-3)}$$

$$\tau_p = \frac{\tau_{RZ}}{p^k}\ (1.5 \le k \le 2) \qquad \text{(V-4)}$$

Here, RT is the gas constant multiplied by the absolute temperature, M and n_s are the molar mass and number of segments (springs) per chain of the polymer, respectively, and τ_{RZ} is the longest relaxation time of the bead-spring model. The value of k in the Rouse-Zimm model indicates the transition from the free-draining limit (k = 2.0) to the non-free-draining limit (k = 1.5).

The stress-optical rule holds between $G_{\mathrm{ornt}}{}^*$ and $K_{\mathrm{ornt}}{}^*$. Thus, one can write

$$K^*_{\mathrm{ornt}} = C_{\mathrm{RZ}} G^*_{\mathrm{ornt}} \qquad \text{(V-5)}$$

with the stress-optical coefficient C_{RZ}. In what follows, $K_{\mathrm{ornt}}{}^*$ is written as $K_{\mathrm{RZ}}{}^*$, corresponding to $G_{\mathrm{ornt}}{}^* = G_{\mathrm{RZ}}{}^*$.

The molar mass of the Rouse segment size, M_{s}, can be estimated from eq V-3 as.

$$M_{\mathrm{s}} = \frac{M}{n_{\mathrm{s}}} = \frac{cRT}{G'_{\mathrm{RZ}}(\infty)} = \frac{C_{\mathrm{RZ}} cRT}{K'_{\mathrm{RZ}}(\infty)} \qquad \text{(V-6)}$$

While G^* contains the $G_{\mathrm{curv}}{}^*$ and $G_{\mathrm{tens}}{}^*$ terms in eq 1, K^* is free from the corresponding modes. Thus, $G_{\mathrm{RZ}}{}^*$ can be determined more easily from $K_{\mathrm{ornt}}{}^*$ and C_{RZ}, without considering the contributions $G_{\mathrm{curv}}{}^*$ and $G_{\mathrm{tens}}{}^*$ in G^*.

V-3-3. The Rouse Segment Size of CTPC in TCP

Figure V-3 compares the frequency dependence of G^* with that of K^*/C_{RZ} for the TCP solution of sample CTPC25K at c = 0.0152 g cm^{-3}. The C_{RZ} value was chosen to be 5.0×10^{-8} for K'/C_{RZ} to agree with G' at $\log(\omega a_{\mathrm{T}}/\mathrm{s}^{-1}) < 2$, where the polymer orientation mode is predominant in both G^* and K^*. The Rouse segment size can be estimated from the plateau of the composite curve for K'/C_{RZ} at $3 < \log(\omega a_{\mathrm{T}}/\mathrm{s}^{-1}) < 4.5$. The limiting modulus due to the polymer orientation contribution at high frequencies, $G'_{\mathrm{RZ}}(\infty) = K'_{\mathrm{RZ}}(\infty)/C_{\mathrm{RZ}}$ was estimated to be ca. 1250 Pa, from which M_{s} was estimated to be 25000 g mol^{-1} by eq V-6. Thus, the number n_{s} of the Rouse segments of this sample is equal to unity.

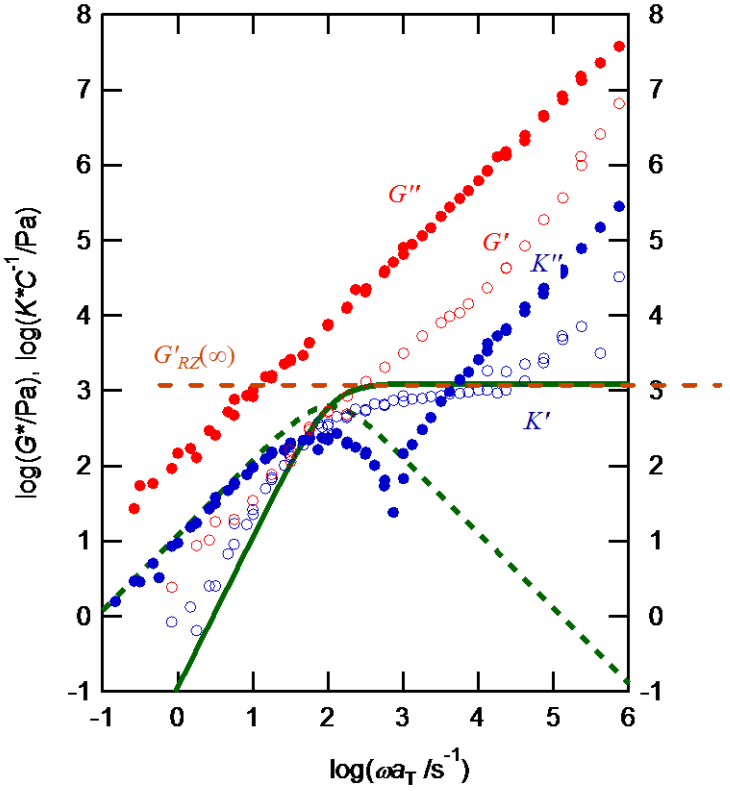

Figure V-3. Frequency dependences of G^* and K^*/C for a TCP solution of CTPC25K sample. Green curves indicate the theoretical values for the Rouse-Zimm theory for K_{RZ}^* and black curves do G_{locl}^*. Reference temperature, T_r, is –25 °C. Concentration, c, is 0.0152g cm^{-3}. The stress optical coefficient, C , is -5.0×10^{-8}Pa^{-1}

Figure V-4 shows G^* and K^*/C_{RZ} for a TCP solution of sample CTPC25K at a higher concentration c = 0.136 g cm^{-3}. Values of C_{RZ} were chosen to be 2.8×10^{-8} Pa^{-1} to obtain the agreement between K'/C_{RZ} and G' at $\log(\omega a_T/s^{-1}) < 0$, where the polymer orientation mode is predominant in both G^* and K^*. The Rouse segment size can be estimated from the plateau of the composite curve for K'/C_{RZ} at $2 < \log(\omega a_T/s^{-1}) < 4$. Limiting moduli due to the polymer

orientation contribution at high frequencies, $G'_{RZ}(\infty) = K'_{RZ}(\infty)/C_{RZ,}$ were estimated to be ca.12600 Pa, from which M_s were estimated to be 22000 g mol^{-1} by eq V-6 for sample CTPC25K at c = 0.136 g cm^{-3}.

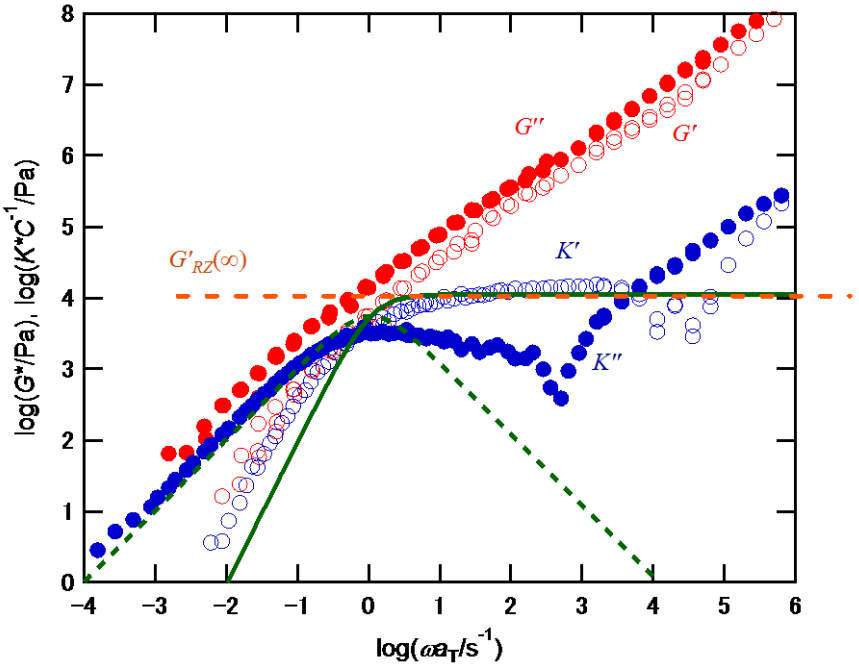

Figure V-4. Frequency dependence of G^* and K^* for a TCP solution of CTPC25K sample. Concentration, c, is 0.136 g cm^{-3}. Green curves indicate the theoretical values for the Rouse-Zimm theory for G_{RZ}^* at n_s = 1 (i.e, the Maxwell model). Reference temperature, T_r, is –25 °C. The stress optical coefficient, C, is -2.8×10^{-8} Pa^{-1}.

The values of M_s for sample CTPC25K at c = 0.0152 g cm^{-3} and 0.136 g cm^{-3} are not so much different. The concentration independence of M_s agrees with the result of cellulose in

BmimCl reported by Maeda et al,[1] but not with the result of Inoue et al.[10] that M_s of polystyrene in TCP sharply decreased with c. The chain backbone structure or chain stiffness may affect the concentration dependence of M_s.

The same comparison between G^* and K^*/C_{RZ} was made for the TCP solution of sample CTPC2040K at c = 0.0228 g cm^{-3} shown in Figure V-2. In Figure V-5, the value of C_{RZ} was chosen to be 1.1×10^{-7} Pa^{-1} to obtain the agreement between K'/C_{RZ} and G' at $\log(\omega a_T/s^{-1}) < 1$, where the polymer orientation mode is predominant, and the limiting modulus due to the polymer orientation contribution at high frequencies, $G'_{RZ}(\infty) = K'_{RZ}(\infty)/C_{RZ}$, was estimated to be 2700 Pa from the plateau of the composite curve for K'/C_{RZ} at $3 < \log(\omega a_T/s^{-1}) < 4.5$ in Figure V-5. The Rouse segment size M_s was estimated to be 17000 g mol^{-1} by eq V-6 for sample CTPC2040K at c = 0.0228 g cm^{-3}.

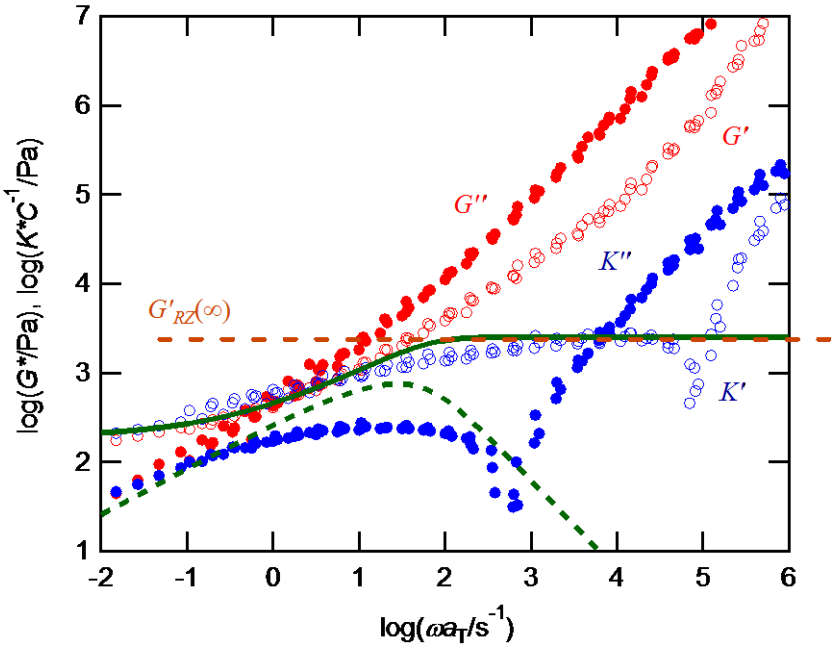

Figure V-5. Frequency dependence of K^* for a TCP solution of CTPC2040K sample. Green curves indicate the theoretical values for the Rouse-Mooney theory for G_{ornt}^*. Reference temperature, T_r, is –25 °C. Concentration, c, is 0.0228 g cm^{-3}. The stress optical coefficient, C, is -1.1×10^{-7}Pa^{-1}.

V-3-4. Viscoelastic Relaxation Spectrum

For sample CTPC25K, the number n_s of the Rouse segment is almost unity, and the viscoelastic relaxation spectrum of the Rouse-Zimm theory, given by eq V-6, reduces to that of the Maxwell model. In Figures V-3 and V-4, green curves show the theoretical values for the Maxwell model (eq V-6 with $n_s = 1$). The theoretical curves almost fit to the experimental results of K^*/C_{RZ} in lower frequency regions.

As already mentioned, the solvent contribution K_e^* to K^* becomes important in high frequency regions. Thus, the deviations of the experimental data from the theoretical green curves are owing to this solvent contribution. The peak of K''/C_{RZ} in Figure V-4 is slightly broader than that in Figure V-3. This broadness would be attributed to the inter-chain interaction.

For the high M sample, CTPC2040K, the number of the Rouse segments n_s is 120, so that the relaxation spectrum of the Rouse-Zimm theory, given by eq V-6 with $k = 2$ is much broader than that of the Maxwell model, as shown by green solid and dashed curves in Figure 5. The experimental results of K^*/C_{RZ} are also broader than those for CTPC25K, being consistent with the theoretical prediction. Deviations of the experimental K'/C_{RZ} and K''/C_{RZ} from the green curves in the high frequency region come from the solvent contribution K_e^*.

V-3-5 Molar Mass between Entanglements for CTPC.

As shown in Figure V-2, G' for a TCP solution of CTPC2040K sample with $c = 0.0228$ g cm^{-3} shows the rubbery plateau due to the entanglement among polymer chains in the low frequency region [$-4 < \log(\omega a_T/s^{-1}) < 0$]. From the rubbery plateau modulus $G_N(c)$ (= 200 Pa), the molar mass between entanglements, $M_e(c) \equiv cRT/G_N(c)$ for CTPC in TCP at $c = 0.0228$ g cm^{-3} is calculated to be 2.4×10^5 g mol^{-1}. The molar mass between entanglements in hypothetical melt, M_e, is roughly estimated to be 5400 g mol^{-1}. This value is considerably

smaller than the Rouse segment size which we have estimated in the previous section. These values indicates that CTPC is rigid chain.

The viscoelastic properties of well-entangled semiflexible chains are not experimentally established. Here, we follow the Morse theory, which predicts the concentration dependence of M_e. The result is illustrated in Figure V-6. We assumed that the molar mass of the Rouse segments is independent of concentration because the previous study strongly suggests that independent segments size for rigid chains. The figure predicts that M_e agrees with M_s around $c \sim 0.17$ g cm^{-3}. At higher concentrations, tightly entangled region will be observed, where M_e is smaller than M_s.

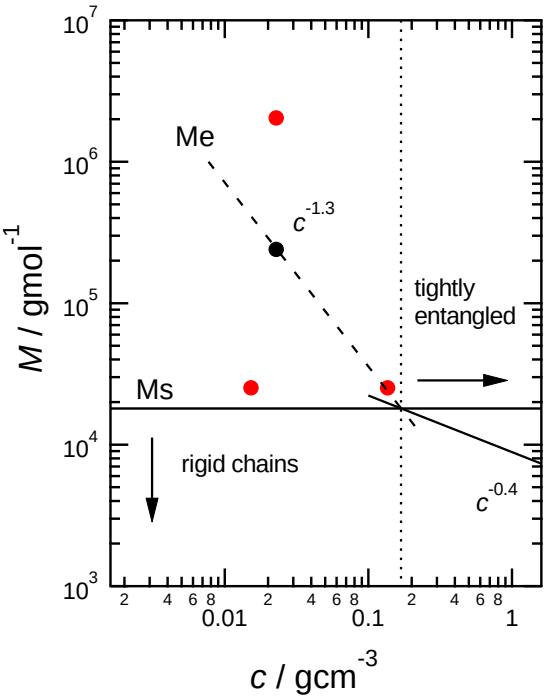

Figure V-6. Concentration dependence of molar mass between entanglements for CTPC in TCP. The red circles are the three CTPC samples. The filled black circle represents the solution examined in the study.

V-4 Conclusions

In this Chapter, the Rouse segment size M_s of a typical semiflexible polymer cellulose tris(phenylcarbamate) (CTPC) in tricresyl phosphate (TCP) was estimated from simultaneous measurements of the dynamic viscoelasticity and birefringence. The results are summarized in Table V-2. Essentially, M_s of CTPC in TCP is independent of the polymer concentration

and molar mass. The polymer concentration independence of M_s was reported also for cellulose in BmimCl by Maeda et al. (cf. Table V-2).

Table V-2. Molecular Characteristics of CTPC and Cellulose Samples Used.

polymer	solvent	molar mass / 10^4 g/mol	c / g/cm^3	K^*/C_{RZ} / 10^3 Pa	M_s / 10^3 g/mol	n_s	n/n_s[a]
CTPC	TCP	2.5	0.0152	1.25	25	1.0	48
CTPC	TCP	2.5	0.136	12.6	22	1.1	43
CTPC	TCP	204	0.0228	2.7	17	120	32
cellulose[b]	BmimCl	1.4	0.0214	19.4	2.3	6.1	14
cellulose[b]	BmimCl	1.4	0.108	96.8			

[a] Number of glucose residues consisting of a Rouse segment.

[b] Data taken from Ref. 1.

The number of glucose residues consisting of a Rouse segment is calculated from $n/n_s = M_s/M_0$, where M_0 is the molar mass per glucose residue. The results are listed in the eighth column of Table V-2. The values of n/n_s for CTPC in TCP are appreciably larger than n/n_s for cellulose in BmimCl. Amelar et al.[11] reported that n/n_s for polystyrene in a Aroclor is as large as 100 at $c < 0.1$ g/cm^3, but later Inoue et al.[10] demonstrated that n/n_s for reduces up to 20 with increasing c. In the next Chapter, M_s for CTPC and other polysaccharides are compared with the Kuhn segment size M_K obtained in Chapters II and IV.

References

1. A. Maeda, T. Inoue, T. Sato *Macromolecules*, **2013**, 46, 7118-7124.

2. S. C. Peterson, I. Echeverria, S. F. Hahn, D. A. Strand, J. L. Schrag, *J. Polym. Sci. B. Polym. Phys* **2001**, 39, 2860-2870.

3. F. Kasabo, T. Kanematsu, T. Nakagawa, T. Sato, A. Teramoto, *Macromolecules* **2000,** 33, 2748-2756.

4. T. Sato, T. Shimizu, F. Kasabo, A. Teramoto, *Macromolecules* **2003,** 36, 2939-2943.

5. D. C. Morse, *Macromolecules*, **1998**, 31, 7044–7067.

6. D. C. Morse, *Macromolecules* **1998,** 31, 7030-7043.

7. V. Shankar, M. Pasquali, D. C. Morse, *J. Rheol.* **2002**, 46, 1111-1154.

8. P. E. Rouse, *J. Chem. Phys*. **1953**, 21, 1272-1280.

9. B. H. Zimm, *J. Chem. Phys.* **1956**, 24, 269-278.

10. T. Inoue, T. Uematsu, K. Osaki, *Macromolecules*, **2002**, 35, 820-826.

11. S. Amelar, C. E. Eastman, R. L. Morris, M. A. Smeltzly, T. P. Lodge, E. D. von Meerwall, *Macromolecules* **1991,** 24, 3505-3516.

Chapter VI.

Summary and Conclusions

VI-1. Introduction

The aim of this thesis work is to investigate the conformation of cellulosic chains and to clarify the relationship between the conformation and dynamics of cellulosic and amylosic chains in solution. Small-angle X-ray scattering measurements were performed for cellulose, amylose, and their derivatives in high-viscosity solvents including ionic liquid to determine the chain stiffness. Furthermore, dynamic viscoelasticity and birefringence have been investigated to clarify the relationship between conformation and dynamics.

VI-2. Conformations of Cellulosic and Amylosic Chains in Solution

In Chapter II, small-angle X-ray scattering measurements were made for cellulose, amylose, and amylose tris(ethylcarbamate) (ATEC) in an ionic liquid [1-butyl-3- methylimidazolium chloride (BmimCl)] at 25 °C to determine *z*-average mean-square radius of gyration $\langle S^2 \rangle_z$ and the particle scattering function $P(q)$. The obtained data were analyzed in terms of the wormlike chain model to estimate the Kuhn segment length λ^{-1} (the stiffness parameter, equivalent to twice of the persistence length) and the helix pitch (or helix rise) per residue h. The chain stiffness (λ^{-1}) was determined to be 7 ± 1 nm for cellulose in BmimCl, 3.5 ± 0.5 nm

for amylose in BmimCl, and 7.5 ± 0.5 nm for ATEC in BmimCl. These values are almost the same or somewhat smaller than those of previously investigated systems, indicating these polymers have relatively high flexibility in the ionic liquid. It is reasonable to suppose that disruption of intramolecular hydrogen bonds of polysaccharide makes the main chain rather flexible in the ionic liquid.

In Chapter III, we prepared cellulose tris(ethylcarbamate) (CTEC), cellulose tris(*n*-butylcarbamate) (CTBC), and cellulose tris(*n*-octadecylcarbamate) (CTODC) samples with different molecular weight to determine their conformational properties in dilute solution. Weight average molar masses M_w, *z*-average mean-square radii of gyration $\langle S^2 \rangle_z$, particle scattering functions $P(q)$, and intrinsic viscosities $[\eta]$ of the CTEC, CTBC, and CTODC samples in tetrahydrofuran (THF) at 25 °C were determined by size exclusion chromatography equipped with multi-angle light scattering detectors (SEC-MALS), small angle X-ray scattering (SAXS), and viscometry. Infrared (IR) absorption measurements were also made to observe intramolecular hydrogen bonding between C=O and NH groups. The obtained $\langle S^2 \rangle_z$, $P(q)$, and $[\eta]$ data were analyzed in terms of the wormlike chain model to determine the Kuhn segment length (stiffness parameter, or twice of the persistence length) λ^{-1} and the helix pitch (rise) per residue *h*. While CTBC has the highest chain stiffness in the three cellulose derivatives as in the case of the corresponding amylose derivatives, the difference in the wormlike chain parameters is less significant for the cellulose alkylcarbamate derivatives. Indeed,

intramolecular hydrogen bonding of CTEC, CTBC, and CTODC is weaker and fewer than that for the corresponding amylose derivatives owing to the main chain linkage, α or β.

Chapter IV described the small-angle X-ray scattering (SAXS) measurements carried out for two cellulose tris(phenylcarbamate) (CTPC) samples in tricresyl phosphate (TCP) at 25 °C. The analysis method is similar to Chapter II. The resultant λ^{-1} and h were 11.5 ± 0.5 nm and 0.51 nm, respectively. While the latter value (h) is consistent with the previously reported values both for cellulose and cellulose derivatives, appreciably higher chain flexibility was found for CTPC in TCP than that in tetrahydrofuran at 25 °C (19 – 24 nm) whereas the value is fairly close to that in anisol, cyclohexanol, and benzophenone if assuming an appropriate temperature coefficient. We may thus conclude that CTPC behaves as a semiflexible chain in TCP and the chain stiffness is relatively small in the previously investigated solvents.

VI-3. Dynamics of a Cellulose Derivative in Ssolution

Chapter V deals with simultaneous measurements of the dynamic viscoelasticity and birefringence, performed on CTPC/TCP systems. From the viscoelasticity and birefringence measurements, the Rouse segment size M_S reflecting the dynamic chain rigidity was estimated to be 18000 - 25000 g mol^{-1} for CTPC in TCP, being essentially independent of the polymer concentration and molar mass.

VI-4. Comparison between the Rouse and Kuhn Segment Sizes

Table VI-1 lists the Rouse segment size M_s and the Kuhn segment size M_K for various polymers in solution, obtained in the present thesis work and previous studies. Here, the M_K values were calculated from λ^{-1}, h, and the molar mass M_0 per main-chain (virtual) bond by $M_K = \lambda^{-1}(M_0/h)$. The ratio of M_s to M_K for CTPC in TCP is 1.7, which is close to but slightly larger than the ratios for cellulose and amylose in BmimCl. As shown in Figure I-6 of Chapter I, the entropic elastic force constant diminishes appreciably at $M_s/M_K = 1.7$ by the chain stiffness effect, and this M_s/M_K value is physically reasonable.

Table VI-1. Comparison between the Kuhn and Rouse Segment Sizes for Various Polymers in Solution.

polymer	solvent	λ^{-1} / nm	b / nm	M_K / 10^3 g mol^{-1}	M_s / 10^3 g mol^{-1}	M_s/M_K
CTPC	TCP	11.5	0.55	12 ± 1	21 ± 4	1.7
cellulose	BmimCl	7	0.55	2.3 ± 0.3	2.3 [a]	1.0
amylose	BmimCl	3.5	0.44	1.8 ± 0.3	2.2 [b]	1.2
polystyrene	Aroclor	2 [c]	0.15	0.83 [c]	5.2 [d]	6.3

[a] Ref. 1. [b] Ref. 2. [c] Ref. 3. [d] Ref. 4.

Table VI-1 includes also the results of M_s and M_K for polystyrene in Aroclor ($c < 0.1$ g/cm3), reported by Amelar et al.[4] As already pointed out by the authors themselves, the Rouse segment size considerably larger than the Kuhn segment size, although the conformational rearrangement of the polystyrene chain must occur on shorter length scales. Later, Inoue et al.[5] reported that the ratio M_s/M_K for polystyrene in TCP decreases with increasing the polymer concentration. Furthermore, Inoue and Osaki[6] demonstrated that M_s values obtained from the rubbery component of Young's modulus at high frequency limit are comparable to M_K for more than ten polymers in bulk, indicating the close relation between the fast dynamics and the chemical structure of polymers.

The polymer chain changes its conformation by the internal rotation of each bond or virtual bond. The bond length b of polystyrene is 0.15 nm, which is much smaller than the molecular size of Aroclor or TCP (ca. 1 nm). In the Aroclor or TCP solution, the micro-Brownian motion of the polystyrene chain must take place along with the molecule motion of the solvent to produce the vacancy in the vicinity of the polymer chain. In other words, when the solvent molecule moves to produce a vacant space near the polymer chain, the micro-Brownian motion of the polymer sub-chain with the comparable size to the solvent size may occur simultaneously. This indicates that the local polymer chain dynamics is determined not only by the polymer chemical structure but also by the solvent molecular size. As listed in Table VI-1, virtual bond lengths of the polysaccharides are considerably larger than b of polystyrene, and differences

between *b* and the solvent molecular size is smaller. Thus, the effect of the solvent molecular size on M_s may be minor. (For bulk polymers, each polymer chain is surrounded by polymer chains with the same *b*, so that the environment effect on M_s may not also be important.)

References

1. A. Maeda, T. Inoue, T. Sato, *Macromolecules* **2013,** *46*, 7118-7124.

2. A. Maeda, Conformation and Dynamics of the Cellulose Chain in Ionic Liquids. Ph.D. Thesis, Osaka University, 2014.

3. T. Norisuye, H. Fujita, *Polym. J.* **1982**, *14*, 143-147.

4. S. Amelar, C. E. Eastman, R. L. Morris, M. A. Smeltzly, T. P. Lodge, E. D. von Meerwall, *Macromolecules* **1991,** 24, 3505-3516.

5. T. Inoue, T. Uematsu, K. Osaki, *Macromolecules*, **2002**, 35, 820-826.

6. T. Inoue, K. Osaki, *Macromolecules*, **1996**, 29, 1595-1599.

List of Publications:

This thesis work has been or will be published in the following papers.

[1] “Dimensional and Hydrodynamic Properties of Cellulose tris(alkylcarbamate)s in Solution: Side Chain Dependent Conformation in Tetrahydrofuran.”

X. Y. Jiang, A. Ryoki, K. Terao *Polymer* **2017**, 112, 152-158.

[2] “Chain Dimensions and Stiffness of Cellulosic and Amylosic Chains in an Ionic Liquid: Cellulose, Amylose, and an Amylose Carbamate in BmimCl”

X.Y. Jiang, S. Kitamura, T. Sato, K. Terao *Macromolecules* in press.

[3] “Chain stiffness of cellulose tris(phenylcarabamate) in tricresyl phosphate (TCP)”

X.Y. Jiang, T. Sato, K. Terao submitted.

Related Paper

[4] “Chain dimensions and intermolecular interactions of polysilanes bearing alkyl side groups over the UV thermochromic temperature.”

X. Y. Jiang, K. Terao, W. J. Chung, M. Naito, *Polymer* **2015**, 68, 221-226.